



Boundary conditions involving pressure for the Stokes problem and applications in computational hemodynamics

Silvia Bertoluzza, Vincent Chabannes, Christophe Prud'Homme, Marcela Szopos

► To cite this version:

Silvia Bertoluzza, Vincent Chabannes, Christophe Prud'Homme, Marcela Szopos. Boundary conditions involving pressure for the Stokes problem and applications in computational hemodynamics. Computer Methods in Applied Mechanics and Engineering, Elsevier, 2017, 10.1016/j.cma.2017.04.024 . hal-01420651v2

HAL Id: hal-01420651

<https://hal.archives-ouvertes.fr/hal-01420651v2>

Submitted on 10 May 2017

HAL is a multi-disciplinary open access archive for the deposit and dissemination of scientific research documents, whether they are published or not. The documents may come from teaching and research institutions in France or abroad, or from public or private research centers.

L'archive ouverte pluridisciplinaire **HAL**, est destinée au dépôt et à la diffusion de documents scientifiques de niveau recherche, publiés ou non, émanant des établissements d'enseignement et de recherche français ou étrangers, des laboratoires publics ou privés.



Distributed under a Creative Commons Attribution - NonCommercial - ShareAlike 4.0 International License

BOUNDARY CONDITIONS INVOLVING PRESSURE FOR THE STOKES PROBLEM AND APPLICATIONS IN COMPUTATIONAL HEMODYNAMICS

S. BERTOLUZZA

CNR - Istituto di Matematica Applicata e Tecnologie Informatiche "Enrico Magenes", v. Ferrata 1, 27100 Pavia (Italy)

V. CHABANNES, C. PRUD'HOMME, M. SZOPOS

Université de Strasbourg, CNRS, IRMA UMR 7501, F-67000 Strasbourg, France

ABSTRACT. Pressure driven flows typically occur in hydraulic networks, *e.g.* oil ducts, water supply, biological flows, microfluidic channels *etc.* However, Stokes and Navier-Stokes problems are most often studied in a framework where Dirichlet type boundary conditions on the velocity field are imposed, thanks to the simpler settings from the theoretical and numerical points of view. In this work, we propose a novel formulation of the Stokes system with pressure boundary condition, together with no tangential flow, on a part of the boundary in a standard Stokes functional framework using Lagrange multipliers to enforce the latter constraint on velocity. More precisely, we carry out *(i)* a complete analysis of the formulation from the continuous to discrete level in two and three dimensions *(ii)* the description of our solution strategy, *(iii)* a verification of the convergence properties with an analytic solution and finally *(iv)* three-dimensional simulations of blood flow in the cerebral venous network that are in line with *in-vivo* measurements and the presentation of some performance metrics with respect to our solution strategy.

1. INTRODUCTION

Stokes and Navier-Stokes problems are often studied in a framework where Dirichlet type boundary conditions on the velocity field are imposed. However, in hydraulic network-like systems, for instance oil ducts, water supply, microfluidic channels or the blood circulatory system, different formulations with boundary conditions involving components of the velocity field, stresses or pressure, are of interest. A recent review of some of the formulations proposed in the literature, and their associated boundary conditions, with a focus on applications to air and blood flows can be found in [17].

In this work, we are motivated by the computational modeling of some biological flows driven by physiological pressure gradients and more precisely we are interested in the case when the velocity field is imposed on one part of the boundary and pressure values are prescribed, together with the condition of no tangential flow, on the remaining part. A variational formulation taking into account this type of boundary conditions was first introduced in the seminal works [29, 6, 11]. A lot of subsequent literature was devoted to this topic. At a continuous level, the well-posedness of the variational formulation both for Stokes and Navier-Stokes systems was investigated in a steady Hilbertian case [11, 20], unsteady nonlinear two-dimensional case [26] and recently extended to L^p -theory for $1 < p < \infty$ in [2]. Several discretization approaches were proposed, including finite differences [24], SPH method [23] or finite elements [12, 20, 5, 7]. Numerical experiments in the finite element framework enforce this type of boundary conditions through a penalty method, for Newtonian [12, 5] and generalized Newtonian fluids [5]. Recent developments concern the Navier-Stokes problem in the context of a simplified fluid-structure model for blood flows [21]. This so-called *Surface Pressure Model* is analyzed in [10].

Key words and phrases. Stokes equations, pressure boundary conditions, finite element method, computational hemodynamics.

Whereas most of the previous contributions expressed the conservation of the momentum in terms of the Laplacian of the velocity, we focus hereafter on the equivalent formulation in terms of the divergence of the symmetric gradient, useful in some applications such as fluid-structure interaction problems. To take into account the non-standard boundary conditions, we introduce a new Lagrange multipliers-based formulation, which we discretize in a finite-element framework. Although we have to deal with supplementary unknowns – which increases the complexity of the problem – this novel formulation allows for several advantages. At a continuous level, the well-posedness of the problem is proved in the same functional spaces as for standard boundary conditions, and includes the case of L^2 pressure boundary data, that was not covered in [7]. The coupling between the velocity and the Lagrange multiplier occurs only on the boundary, and no parameters need to be chosen, as when enforcing the constraint through a penalty method [12, 5]. Moreover, the discrete analysis allows us to obtain optimal convergence rates for standard inf-sup stable finite element spaces, without requiring **curl** conforming finite elements [20] or stabilized formulations [7].

Another interesting feature of the proposed formulation comes from its ability to properly handle the prescription of inlet/outlet boundary conditions at artificial boundaries. This situation may occur for instance when modeling flow through a network of pipes truncated to a region of interest. The challenging issue of prescribing suitable boundary conditions at the artificial sections is reviewed in [16] and different strategies to cope with this difficulty are proposed for instance in [35] by means of the Nitsche method or in [30] in the context of blood flow modeling. Moreover, as noted in [25, 22], using the symmetric gradient $\frac{1}{2}(\nabla \mathbf{u} + \nabla \mathbf{u}^T)$ and prescribing the normal stress at the outlet lead to a non-physical representation of the flow: the velocity vectors “spread” like at the end of a pipe, instead of mimicking the fact that the network continues after this artificial section. Alternatively, the non symmetric tensor $\nabla \mathbf{u}$ can be used to recover the Poiseuille exact solution in a cylinder, but the physical meaning of such a boundary condition is not clear. In the present work, the mathematical and computational models share both advantages: the fluid model is described in terms of the mechanical stress tensor, which is more appropriate from the modeling viewpoint, and it is able to properly take into account the fact that the flow continues beyond the boundaries, thanks to the specific form of the boundary conditions.

The remainder of the article is organized as follows. Section 2 is devoted to the description of the Lagrange multiplier-based variational formulation of the problem and its analysis at a continuous level and Section 3 to the discrete counterpart of the analysis. Section 4 describes the numerical and computational procedure and results are presented in Section 5. Concluding remarks and some perspectives are gathered in the final section.

2. THE CONTINUOUS PROBLEM

2.1. General framework. Let $\Omega \subset \mathbb{R}^d$, $d = 2, 3$ be a bounded domain and denote by $\partial\Omega$ its boundary. We consider hereafter the steady state of a viscous incompressible fluid at low Reynolds number, described by the velocity and pressure fields \mathbf{u} and p that satisfy the following Stokes equations:

$$(2.1) \quad -2\mu \nabla \cdot (\mathbf{D}(\mathbf{u})) + \nabla p = \rho \mathbf{f}, \quad \text{in } \Omega,$$

$$(2.2) \quad \nabla \cdot \mathbf{u} = 0, \quad \text{in } \Omega,$$

$$(2.3) \quad \mathbf{u} = 0, \quad \text{on } \Gamma_1,$$

$$(2.4) \quad \mathbf{u} \times \mathbf{n} = 0, \quad \text{on } \Gamma_2, \text{ and}$$

$$(2.5) \quad p = p_0, \quad \text{on } \Gamma_2,$$

where

$$\partial\Omega = \bar{\Gamma}_1 \cup \bar{\Gamma}_2, \quad \text{with } \Gamma_1 \cap \Gamma_2 = \emptyset \quad \text{and such that each connected component of } \Gamma_2 \text{ is flat,}$$

represents a partition without overlap of the boundary of Ω and \mathbf{n} indicates the outward normal to $\partial\Omega$. The notation $\mathbf{D}(\mathbf{u}) = \frac{1}{2}(\nabla \mathbf{u} + \nabla \mathbf{u}^T)$ designates the strain rate tensor, μ and ρ are the dynamic viscosity and the density of the fluid, respectively, the function \mathbf{f} is a given external force and the function p_0 a given pressure.

As an example of a real-world problem for which one of the main mechanisms driving the flow is the pressure drop, we consider the hemodynamics modeling of the cerebral venous network presented in Fig. 1. The complex realistic three-dimensional description was constructed in the framework of the AngloTkProject [1] from 3D

angiographic images obtained by magnetic resonance angiography. Blood from the microcirculation enters the network through input veins, like the superior cerebral veins (1), internal cerebral vein (4), basal vein (5) etc.; it flows through the superior sagittal sinus (2) and the straight sinus (3), down to the confluence of sinuses (6). Next, it passes into the left, respectively right, transverse sinus (7) and sigmoid sinus (8), to finally reach the extracranial region through the draining vessels (9), [33].

A computational model based on the assumptions that at this scale blood can be considered as an incompressible, homogeneous, Newtonian fluid, leads to the description of the flow by means of the Navier-Stokes equations [27] in a fixed domain. Body forces contribution (for instance gravity), can be incorporated in the model through the right-hand side term and walls are assumed to be rigid. In practice, velocity information in the cerebral veins is not collected from routine clinical examinations, hence an alternative is to impose a pressure gradient by means of specified pressures at the inflow and outflow boundaries. Consequently, in a first approximation for low Reynolds numbers, the problem takes the form (2.1 - 2.5), with Γ_1 corresponding to the lateral boundary (the vessel wall) and Γ_2 to the union of the 29 inflow and 2 outflow sections, where pressure values can be prescribed, together with the condition of no tangential flow.

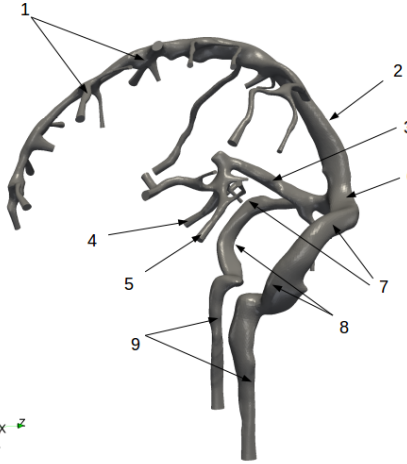


FIGURE 1. Cerebral venous network.

Remark 2.1. Previous works [29, 6, 11, 12, 7] classically take into account non standard boundary conditions of type (2.3 - 2.5) by expressing the conservation of the momentum in terms of the Laplacian of the velocity and then using as a key ingredient the rotational formulation for the equation, based on:

$$-\Delta \mathbf{u} = \nabla \times (\nabla \times \mathbf{u}) - \nabla(\nabla \cdot \mathbf{u}).$$

Although at a continuous level the two formulations are equivalent, since

$$\nabla \cdot \mathbf{u} = 0 \Rightarrow \nabla \cdot (\nabla \mathbf{u} + \nabla \mathbf{u}^T) = \Delta \mathbf{u},$$

from a modeling standpoint it may be useful to work with the symmetric tensor. For instance, in fluid-structure problems, formulation (2.1 - 2.5) gives directly the natural boundary condition for the structure problem in terms of the force exerted by the fluid on its boundary.

2.2. The Lagrange multiplier formulation. Let us first introduce some notations. In the following we will write $A \lesssim B$ (resp. $A \gtrsim B$) to indicate that there exists a constant $c > 0$ which might depend on Ω , Γ and Γ_2 , as well as on μ , but independent of the meshsize parameter h that will be introduced in Section 3, such that $A \leq cB$, (resp. $A \geq cB$). We will write $A \simeq B$ for $A \lesssim B \lesssim A$.

In the following we will deal with both scalar and vector functions in different Sobolev spaces defined on different domains. For a scalar function ϕ defined in a domain $\hat{\Omega}$ ($\hat{\Omega}$ being either one of Ω , Γ or Γ_2), we denote by $\|\phi\|_{s,\hat{\Omega}}$ the $H^s(\hat{\Omega})$ norm. For a vector function $\phi \in [H^s(\hat{\Omega})]^n$ (n either equals to d or $d - 1$) we denote by $\|\phi\|_{s,\hat{\Omega}}$ the $[H^s(\hat{\Omega})]^n$ norm.

Let $\mathbf{f} \in [L^2(\Omega)]^d$ and $p_0 \in L^2(\Omega)$. With the aim of taking into account the boundary conditions (2.3 - 2.5), we first introduce the standard spaces $\mathbf{V} = \{\mathbf{v} \in [H^1(\Omega)]^d : \mathbf{v} = \mathbf{0} \text{ on } \Gamma_1\}$ and $M = L^2(\Omega)$. After multiplying equation (2.1) by $\mathbf{v} \in \mathbf{V}$, we obtain, using integration by parts, the following identity:

$$(2.6) \quad 2\mu \int_{\Omega} \mathbf{D}(\mathbf{u}) : \mathbf{D}(\mathbf{v}) dx - \int_{\Gamma_2} \sigma(\mathbf{u}, p) \mathbf{n} \cdot \mathbf{v} ds - \int_{\Omega} p \nabla \cdot \mathbf{v} dx = \rho \int_{\Omega} \mathbf{f} \cdot \mathbf{v} dx, \forall \mathbf{v} \in \mathbf{V},$$

with

$$\sigma(\mathbf{u}, p) = -p\mathbb{I} + 2\mu\mathbf{D}(\mathbf{u}),$$

where \mathbb{I} denotes the d -dimensional identity matrix, and where we used the identity

$$\sum_{i,j=1}^d D_{ij}(\mathbf{u}) \frac{\partial v_i}{\partial x_j} = \sum_{i,j=1}^d D_{ij}(\mathbf{u}) D_{ij}(\mathbf{v}),$$

which is a consequence of the symmetry of $\mathbf{D}(\mathbf{u})$.

By using a standard integration by parts argument, we can prove the following lemma.

Lemma 2.2. *Let $\mathbf{u} \in [H^1(\Omega)]^d$ ($d = 2, 3$), with $\nabla \cdot \mathbf{D}(\mathbf{u}) \in [L^2(\Omega)]^d$ and with $\nabla \cdot \mathbf{u} = 0$. Then $\mathbf{D}(\mathbf{u})\mathbf{n} \in [H^{-1/2}(\Gamma_2)]^d$.*

We now recall the following theorem.

Theorem 2.3. ([5, Theorem1]) *For any velocity normal surface $\Gamma \subset \partial\Omega$, the normal component of the normal traction is given by*

$$(\sigma(\mathbf{u}, p)\mathbf{n}) \cdot \mathbf{n} = -(p + 2\mu|\mathbf{u}|\kappa),$$

where κ is the mean curvature of Γ . Furthermore, in the case where Γ is a planar surface, this reduces to the pressure condition

$$(\sigma(\mathbf{u}, p)\mathbf{n}) \cdot \mathbf{n} = -p.$$

This leads us to split the contribution of $\sigma(\mathbf{u}, p)\mathbf{n}$ as the sum of a normal component and of a tangential component

$$(2.7) \quad \sigma(\mathbf{u}, p)\mathbf{n} = \nu(\mathbf{u}, p) + \tau(\mathbf{u}, p)$$

with

$$\nu(\mathbf{u}, p) = ((\sigma(\mathbf{u}, p)\mathbf{n}) \cdot \mathbf{n}) \mathbf{n}, \quad \tau(\mathbf{u}, p) = \sigma(\mathbf{u}, p)\mathbf{n} - \nu(\mathbf{u}, p) = ((\sigma(\mathbf{u}, p)\mathbf{n}) \cdot \mathbf{t}) \mathbf{t},$$

where \mathbf{t} is a suitably chosen unit vector, orthogonal to \mathbf{n} . Remark that in three dimensions we have

$$\tau(\mathbf{u}, p) = \mathbf{n} \times (\sigma(\mathbf{u}, p)\mathbf{n}) \times \mathbf{n}.$$

We now observe that (2.4) implies that the planar surface Γ_2 is indeed normal to the velocity. Then, on Γ_2 $\sigma(\mathbf{u}, p)\mathbf{n}$ takes the form

$$(2.8) \quad \sigma(\mathbf{u}, p)\mathbf{n} = -p\mathbf{n} + \tau(\mathbf{u}, p).$$

Using (2.5), and introducing a Lagrange multiplier $\theta = \tau(\mathbf{u}, p)$, the identity (2.6) becomes

$$(2.9) \quad \begin{aligned} 2\mu \int_{\Omega} \mathbf{D}(\mathbf{u}) : \mathbf{D}(\mathbf{v}) dx - \int_{\Omega} p \nabla \cdot \mathbf{v} dx \\ + \int_{\Gamma_2} p_0 \mathbf{n} \cdot \mathbf{v} ds - \int_{\Gamma_2} \theta \cdot \mathbf{v} ds = \rho \int_{\Omega} \mathbf{f} \cdot \mathbf{v} dx, \forall \mathbf{v} \in \mathbf{V}. \end{aligned}$$

As usual, multiplying equation (2.2) by q and integrating over Ω , we obtain

$$(2.10) \quad \int_{\Omega} q \nabla \cdot \mathbf{u} dx = 0, \forall q \in M.$$

In order to impose $\mathbf{u} \times \mathbf{n} = \mathbf{0}$ on Γ_2 we start by observing that, letting $\mathbf{u}_{\parallel} = \mathbf{u} - (\mathbf{u} \cdot \mathbf{n})\mathbf{n}$ denote the tangential component of \mathbf{u} we have

$$\mathbf{u} \times \mathbf{n} = \mathbf{0} \Leftrightarrow \mathbf{u}_{\parallel} = \mathbf{0} \Leftrightarrow \mathbf{u} \cdot \mathbf{t} = 0, \text{ for all unitary vectors } \mathbf{t} \text{ with } \mathbf{t} \cdot \mathbf{n} = 0.$$

We observe that $\mathbf{u} \rightarrow \mathbf{u}|_{\Gamma_2}$ is bijective from $\mathbf{V} \rightarrow [H_{00}^{1/2}(\Gamma_2)]^d$, whose dual is $[H^{-1/2}(\Gamma_2)]^d$. We therefore introduce the space \mathbf{T} defined as

$$\mathbf{T} = \left\{ \zeta \in [H^{-1/2}(\Gamma_2)]^d : \zeta \cdot \mathbf{n} = 0 \right\}.$$

The tangential component of \mathbf{u} vanishes if and only if for all $\zeta \in \mathbf{T}$, we have $\int_{\Gamma_2} \mathbf{u} \cdot \zeta \, dx = 0$. Consequently, we can write the problem in the following double saddle point form: find $\mathbf{u} \in \mathbf{V}, p \in M, \boldsymbol{\theta} \in \mathbf{T}$ such that for all $\mathbf{v} \in \mathbf{V}, q \in M, \zeta \in \mathbf{T}$

$$(2.11) \quad 2\mu \int_{\Omega} \mathbf{D}(\mathbf{u}) : \mathbf{D}(\mathbf{v}) \, dx - \int_{\Omega} p \nabla \cdot \mathbf{v} \, dx - \int_{\Gamma_2} \mathbf{v} \cdot \boldsymbol{\theta} \, dx = \rho \int_{\Omega} \mathbf{f} \cdot \mathbf{v} \, dx - \int_{\Gamma_2} p_0 \mathbf{n} \cdot \mathbf{v} \, ds$$

$$(2.12) \quad \int_{\Omega} q \nabla \cdot \mathbf{u} \, dx = 0$$

$$(2.13) \quad \int_{\Gamma_2} \mathbf{u} \cdot \zeta \, dx = 0,$$

where, by abuse of notation, we indicate with the integral sign the duality relation between $[H_{00}^{1/2}(\Gamma_2)]^d$ and $[H^{-1/2}(\Gamma_2)]^d$ (remark that such a duality reduces to the $L^2(\Gamma_2)$ scalar product whenever the $H^{-1/2}$ function is in $L^2(\Gamma_2)$, which holds true in particular for functions in the spaces used in the discretization method presented later on).

We next observe that there exists an isomorphism $i : [H^{-1/2}(\Gamma_2)]^{d-1} \rightarrow \mathbf{T}$, whose form will be specified for $d = 2, 3$ in the sequel. Letting then $\Lambda = [H^{-1/2}(\Gamma_2)]^{d-1}$ and introducing the bilinear form $c : \mathbf{V} \times \Lambda \rightarrow \mathbb{R}$ defined as

$$c(\mathbf{u}, \boldsymbol{\lambda}) = \int_{\Gamma_2} \mathbf{u} \cdot i(\boldsymbol{\lambda}) \, dx$$

we can finally write our problem as follows:

Problem 2.4. Find $\mathbf{u} \in \mathbf{V}, p \in M, \boldsymbol{\lambda} \in \Lambda$ such that for all $\mathbf{v} \in \mathbf{V}, q \in M, \boldsymbol{\eta} \in \Lambda$

$$(2.14) \quad 2\mu \int_{\Omega} \mathbf{D}(\mathbf{u}) : \mathbf{D}(\mathbf{v}) \, dx - \int_{\Omega} p \nabla \cdot \mathbf{v} \, dx - c(\mathbf{v}, \boldsymbol{\lambda}) = \rho \int_{\Omega} \mathbf{f} \cdot \mathbf{v} \, dx - \int_{\Gamma_2} p_0 \mathbf{n} \cdot \mathbf{v} \, ds$$

$$(2.15) \quad \int_{\Omega} q \nabla \cdot \mathbf{u} \, dx = 0$$

$$(2.16) \quad c(\mathbf{u}, \boldsymbol{\eta}) = 0.$$

We have the following theorem:

Theorem 2.5. Problem 2.4 admits a unique solution $(\mathbf{u}, p, \boldsymbol{\lambda})$ which verifies

$$\|\mathbf{u}\|_{1,\Omega} + \|p\|_{0,\Omega} + \|\boldsymbol{\lambda}\|_{-1/2,\Gamma_2} \lesssim \|\mathbf{f}\|_{\mathbf{V}'} + \inf_{\mathbf{v} \in \mathbf{V}} \frac{\int_{\Gamma_2} p_0 \mathbf{n} \cdot \mathbf{v} \, ds}{\|\mathbf{v}\|_{1,\Omega}} \lesssim \|\mathbf{f}\|_{0,\Omega} + \|p_0\|_{0,\Gamma_2}.$$

Moreover, if $\mathbf{u} \in [C^2(\Omega)]^d, p \in C^1(\Omega)$, then (\mathbf{u}, p) is the solution of (2.1–2.5) and $\boldsymbol{\lambda}$ verifies

$$i(\boldsymbol{\lambda}) = \tau(\mathbf{u}, p).$$

Before proceeding to prove that Theorem 2.5 holds true let us give some more detail on how the bilinear form c is built in practice in two and three dimensions, by making explicit the isomorphism between \mathbf{T} and Λ .

The two dimensional case. Let $\mathbf{n} = (n_1, n_2)$ denote the unitary normal to Γ_2 and let $\mathbf{t} = (n_2, -n_1)$. Any vector field \mathbf{v} can be written as

$$\mathbf{v} = (\mathbf{v} \cdot \mathbf{n})\mathbf{n} + (\mathbf{v} \cdot \mathbf{t})\mathbf{t}.$$

Any function in \mathbf{T} then has the form $\lambda\mathbf{t}$, with $\lambda \in H^{-1/2}(\Gamma_2)$. The isomorphism i can be written as:

$$i(\lambda) = \lambda\mathbf{t},$$

and we have

$$c(\mathbf{v}, \lambda) = \int_{\Gamma_2} \lambda \mathbf{t} \cdot \mathbf{v} \, ds.$$

The three dimensional case. Letting this time $\mathbf{n} = (n_1, n_2, n_3)$, and assuming, to fix the ideas, that $n_3 \neq 1$, we set

$$\mathbf{t}_1 = \alpha \begin{pmatrix} n_2 \\ -n_1 \\ 0 \end{pmatrix}, \quad \mathbf{t}_2 = \alpha \begin{pmatrix} n_1 n_3 \\ n_2 n_3 \\ n_3^2 - 1 \end{pmatrix}, \quad \text{with } \alpha = (1 - n_3^2)^{-1/2}.$$

The two orthogonal unit vectors \mathbf{t}_1 and \mathbf{t}_2 span the tangential space to Γ_2 . The isomorphism $i : \Lambda \rightarrow \mathbf{T}$ now takes the form

$$i(\lambda) = \lambda_1 \mathbf{t}_1 + \lambda_2 \mathbf{t}_2.$$

The tangential component \mathbf{u}_{\parallel} vanishes if and only if for all $\lambda \in \Lambda$

$$c(\mathbf{u}, \lambda) = \int_{\Gamma_2} (\mathbf{u} \cdot \mathbf{t}_1) \lambda_1 \, ds + \int_{\Gamma_2} (\mathbf{u} \cdot \mathbf{t}_2) \lambda_2 \, ds = 0.$$

Observe that, for $\mathbf{u} = (u_1, u_2, u_3)$ we have

$$\mathbf{u} \cdot \mathbf{t}_1 = \alpha(u_1 n_2 - u_2 n_1), \quad \mathbf{u} \cdot \mathbf{t}_2 = \alpha[(u_1 n_3 - u_3 n_1)n_1 + (u_2 n_3 - u_3 n_2)n_2].$$

Then the bilinear form $c : \mathbf{V} \times \Lambda \rightarrow \mathbb{R}$ can also be written as

$$c(\mathbf{u}, \lambda) = \int_{\Gamma_2} (\mathbf{u} \times \mathbf{n}) \cdot C\lambda \, ds, \quad \text{with } C = \alpha \begin{pmatrix} 0 & n_2 \\ 0 & -n_1 \\ 1 & 0 \end{pmatrix}.$$

2.3. Proof of Theorem 2.5. Following Theorem 1.1, Section II.1 of [8], in order to prove the well posedness of our problem it is sufficient to prove

(1) that an inf-sup condition of the form

$$(2.17) \quad \inf_{\lambda \in \Lambda} \sup_{\mathbf{u} \in \mathbf{V}} \frac{c(\mathbf{u}, \lambda)}{\|\mathbf{u}\|_{1,\Omega} \|\lambda\|_{-1/2, \Gamma_2}} \gtrsim 1$$

holds;

(2) that the problem of finding $(\mathbf{u}, p) \in \mathbf{V}^0 \times M$ such that for all $(\mathbf{v}, q) \in \mathbf{V}^0 \times M$

$$(2.18) \quad a(\mathbf{u}, p; \mathbf{v}, q) = 2\mu \int_{\Omega} \mathbf{D}(\mathbf{u}) : \mathbf{D}(\mathbf{v}) \, dx - \int_{\Omega} p \nabla \cdot \mathbf{v} \, dx + \int_{\Omega} q \nabla \cdot \mathbf{u} \, dx = F(\mathbf{v}, q)$$

is well posed, where \mathbf{V}^0 denotes the kernel of the bilinear form c that is

$$\mathbf{V}^0 = \{\mathbf{u} \in \mathbf{V} : \mathbf{u}_{\parallel} = \mathbf{0}, \text{ on } \Gamma_2\}.$$

Remark that (2.18) is itself a saddle point problem, so, since by Korn inequality the bilinear form

$$2\mu \int_{\Omega} \mathbf{D}(\mathbf{u}) : \mathbf{D}(\mathbf{v}) \, dx$$

is coercive on \mathbf{V} , proving its well posedness also reduces to proving an inf-sup condition, this time of the form

$$\inf_{p \in M} \sup_{\mathbf{u} \in \mathbf{V}^0} \frac{\int_{\Omega} p \nabla \cdot \mathbf{u} \, dx}{\|\mathbf{u}\|_{1,\Omega} \|p\|_{0,\Omega}} \gtrsim 1.$$

Lemma 2.6. *The inf-sup condition (2.17) holds true.*

Proof. In 2D this is easy. It is enough to observe that $\mathbf{V} \times \mathbf{n} = \{\eta \mathbf{t}, \eta \in H_{00}^{1/2}(\Gamma_2)\}$ and that $H_{00}^{1/2}(\Gamma_2)$ is the dual of $H^{-1/2}(\Gamma_2)$. In 3D it is basically the same. We have

$$\begin{pmatrix} \mathbf{u} \cdot \mathbf{t}_1 \\ \mathbf{u} \cdot \mathbf{t}_2 \\ \mathbf{u} \cdot \mathbf{n} \end{pmatrix} = B \begin{pmatrix} u_1 \\ u_2 \\ u_3 \end{pmatrix} \quad \text{with} \quad B = \begin{pmatrix} \alpha n_2 & -\alpha n_1 & 0 \\ \alpha n_3 n_1 & \alpha n_2 n_3 & \alpha(n_3^2 - 1) \\ n_1 & n_2 & n_3 \end{pmatrix}.$$

Remark that B is a unitary matrix, and then $B^{-1} = B^T$. This immediately gives the inversion formula

$$\begin{pmatrix} u_1 \\ u_2 \\ u_3 \end{pmatrix} = \begin{pmatrix} \alpha n_2 & \alpha n_3 n_1 & n_1 \\ -\alpha n_1 & \alpha n_2 n_3 & n_2 \\ 0 & \alpha(n_3^2 - 1) & n_3 \end{pmatrix} \begin{pmatrix} \mathbf{u} \cdot \mathbf{t}_1 \\ \mathbf{u} \cdot \mathbf{t}_2 \\ \mathbf{u} \cdot \mathbf{n} \end{pmatrix}.$$

We observe that the operators $\mathbf{u} \rightarrow B\mathbf{u}$ and $\mathbf{u} \rightarrow B^T\mathbf{u}$ are bounded from $[H_{00}^{1/2}(\Omega)]^3$ to $[H_{00}^{1/2}(\Omega)]^3$.

Let then $\boldsymbol{\lambda} \in \Lambda$. The duality between $H_{00}^{1/2}(\Gamma_2)$ and $H^{-1/2}(\Gamma_2)$ implies the validity of the inf-sup condition

$$(2.19) \quad \inf_{\boldsymbol{\lambda} \in \Lambda} \sup_{\boldsymbol{\eta} \in [H_{00}^{1/2}(\Gamma_2)]^2} \frac{\int_{\Gamma_2} \boldsymbol{\lambda} \cdot \boldsymbol{\eta} \, ds}{\|\boldsymbol{\lambda}\|_{-1/2, \Gamma_2} \|\boldsymbol{\eta}\|_{[H_{00}^{1/2}(\Gamma_2)]^2}} \gtrsim 1,$$

We then know that there exists $\boldsymbol{\eta} \in [H_{00}^{1/2}(\Gamma_2)]^2$ such that

$$\frac{\int_{\Gamma_2} \boldsymbol{\eta} \cdot \boldsymbol{\lambda} \, ds}{\|\boldsymbol{\eta}\|_{[H_{00}^{1/2}(\Gamma_2)]^2}} \gtrsim \|\boldsymbol{\lambda}\|_{-1/2, \Gamma_2}.$$

Let $\mathbf{u} \in [H^1(\Omega)]^3$ be the solution of

$$-\Delta \mathbf{u} = \mathbf{0}, \quad \mathbf{u} = \mathbf{0} \text{ on } \Gamma_1, \quad \mathbf{u} = B^T \begin{pmatrix} \eta_1 \\ \eta_2 \\ 0 \end{pmatrix} \text{ on } \Gamma_2.$$

We have

$$\|\mathbf{u}\|_{1,\Omega} \simeq \|\mathbf{u}\|_{1/2,\Gamma} \simeq \|\mathbf{u}\|_{[H_{00}^{1/2}(\Gamma_2)]^3} \simeq \|B\mathbf{u}\|_{[H_{00}^{1/2}(\Gamma_2)]^3} = \|\boldsymbol{\eta}\|_{[H_{00}^{1/2}(\Gamma_2)]^2}.$$

Moreover we have

$$c(\mathbf{u}, \boldsymbol{\lambda}) = \int_{\Gamma_2} (\mathbf{u} \cdot \mathbf{t}_1) \lambda_1 \, ds + \int_{\Gamma_2} (\mathbf{u} \cdot \mathbf{t}_2) \lambda_2 \, ds = \int_{\Gamma_2} \boldsymbol{\eta} \cdot \boldsymbol{\lambda} \, ds.$$

Then

$$\frac{c(\mathbf{u}, \boldsymbol{\lambda})}{\|\mathbf{u}\|_{1,\Omega}} \simeq \frac{\int_{\Gamma_2} \boldsymbol{\eta} \cdot \boldsymbol{\lambda} \, ds}{\|\boldsymbol{\eta}\|_{[H_{00}^{1/2}(\Gamma_2)]^2}} \gtrsim \|\boldsymbol{\lambda}\|_{-1/2, \Gamma_2}.$$

□

Lemma 2.7. *We have*

$$\inf_{p \in M} \sup_{\mathbf{u} \in \mathbf{V}^0} \frac{\int_{\Omega} p \nabla \cdot \mathbf{u} \, dx}{\|\mathbf{u}\|_{1,\Omega} \|p\|_{0,\Omega}} \gtrsim 1.$$

Proof. Let $p = p^0 + \bar{p} \in M$, with p^0 with zero average and \bar{p} constant. We let $\mathbf{u}^0 \in [H_0^1(\Omega)]^d$ be such that

$$\int_{\Omega} p^0 \nabla \cdot \mathbf{u}^0 \, dx \geq \|p^0\|_{0,\Omega}^2, \quad \|\mathbf{u}^0\|_{1,\Omega} \simeq \|p^0\|_{0,\Omega}.$$

Such a function exists in view of the inf-sup condition for the continuous Stokes problem with Dirichlet boundary conditions. Let $\bar{\mathbf{u}} \in [H^2(\Omega)]^d$ be a fixed harmonic function with

$$\bar{\mathbf{u}} = \mathbf{0} \text{ on } \Gamma_1, \quad \bar{\mathbf{u}} \times \mathbf{n} = \mathbf{0} \text{ on } \Gamma_2, \quad \int_{\Gamma_2} \bar{\mathbf{u}} \cdot \mathbf{n} \, ds = 1.$$

Note that the H^2 regularity of the function $\bar{\mathbf{u}}$ is not mandatory here, but it will be subsequently needed in the proof of Lemma 3.5. We control p with $\mathbf{u} = \mathbf{u}^0 + t\bar{p}\bar{\mathbf{u}}$, where $t > 0$ is a parameter to be chosen later. We have

$$\begin{aligned} \int_{\Omega} (p^0 + \bar{p}) \nabla \cdot (\mathbf{u}^0 + t\bar{p}\bar{\mathbf{u}}) dx &= \int_{\Omega} p^0 \nabla \cdot \mathbf{u}^0 dx + t\bar{p} \int_{\Omega} p^0 \nabla \cdot \bar{\mathbf{u}} dx + t\bar{p}^2 \int_{\Omega} \nabla \cdot \bar{\mathbf{u}} dx = \\ \int_{\Omega} p^0 \nabla \cdot \mathbf{u}^0 dx + t\bar{p} \int_{\Omega} p^0 \nabla \cdot \bar{\mathbf{u}} dx + t\bar{p}^2 \int_{\Gamma_2} \bar{\mathbf{u}} \cdot \mathbf{n} ds &\geq \|p^0\|_{0,\Omega}^2 - \beta_0 t |\bar{p}| \|p^0\|_{0,\Omega} + t\bar{p}^2 \geq \\ \|p^0\|_{0,\Omega}^2 + t\bar{p}^2 - \beta_0 t \frac{1}{2\varepsilon} \|p^0\|_{0,\Omega}^2 - \beta_0 t \frac{\varepsilon}{2} \bar{p}^2, \end{aligned}$$

where $\beta_0 > 0$ is a fixed constant only depending on $\bar{\mathbf{u}}$. We now choose ε in such a way that $\beta_1 = 1 - \beta_0\varepsilon/2 > 0$. Once ε is chosen we choose $t > 0$ in such a way that $\beta_2 = 1 - \beta_0 t/(2\varepsilon) > 0$. We then obtain

$$\int_{\Omega} (p^0 + \bar{p}) \nabla \cdot (\mathbf{u}^0 + t\bar{p}\bar{\mathbf{u}}) dx \geq \beta_2 \|p^0\|_{0,\Omega}^2 + t\beta_1 \bar{p}^2 \gtrsim \|p\|_{0,\Omega}^2.$$

Observing that $\|\mathbf{u}\|_{1,\Omega} \lesssim \|p\|_{0,\Omega}$ we get the desired inf-sup condition. \square

The proof of Theorem 2.5 now follows easily. Existence, uniqueness and stability are simply a consequence of Theorem 1.1, [8] (Section II.1). If \mathbf{u} and p are sufficiently smooth, by a classical argument we obtain (2.1–2.5) almost everywhere by using suitable test functions, and repeating the integration by parts process backwards.

Remark 2.8. It is clear that the Lagrange multiplier formulation described in Problem 2.4 is less straightforward to use in practice, since it introduces supplementary unknowns that increase the complexity of the numerical solution. Nevertheless, this novel formulation allows for pressure boundary conditions with L^2 regularity on the boundary. This result was believed possible but was not covered by the analysis in [7], as explained in the discussion of Sec. 6. Moreover, while the previous treatment of the Laplacian expressed by a rotational formulation required more regularity on the pressure and a velocity field with smooth **curl** and **div** components [11, 20, 7], Theorem 2.5 proves the existence of a solution to the Stokes problem (2.1–2.5) in the same $H^1 \times L^2$ functional spaces as for standard boundary conditions.

3. DISCRETIZATION

We turn now to the discretization of Problem 2.4. Throughout this section we will consider the more challenging three dimensional case, and leave the easier two dimensional case to the reader. We start by introducing a compatible tessellation \mathcal{T}_h of the domain Ω in tetrahedral or hexahedral elements. We assume that the tessellation \mathcal{T}_h is shape regular and quasi uniform, and that it is compatible with the splitting of $\partial\Omega$ into $\Gamma_1 \cup \Gamma_2$, and, more precisely, that, given any element $K \in \mathcal{T}_h$ with $K \cap \Gamma \neq \emptyset$ we either have $K \cap \Gamma \subset \bar{\Gamma}_1$ or $K \cap \Gamma \subset \bar{\Gamma}_2$, so that \mathcal{T}_h induces a proper compatible decomposition of Γ_2 . On \mathcal{T}_h , we introduce piecewise polynomial spaces $\mathbf{V}_h \subseteq \mathbf{V}$, $Q_h \subset M$, respectively approximating velocity and pressure, and we assume that such spaces satisfy the standard inf-sup condition

$$(3.1) \quad \inf_{p_h \in Q_h^0} \sup_{\mathbf{u}_h \in \mathbf{V}_h \cap [H_0^1(\Omega)]^3} \frac{\int_{\Omega} p_h \nabla \cdot \mathbf{u}_h dx}{\|\mathbf{u}_h\|_{1,\Omega} \|p_h\|_{0,\Omega}} \gtrsim 1.$$

(where $Q_h^0 = \{q_h \in Q_h : \int_{\Omega} q_h = 0\}$), so that they provide a stable discretization of the Stokes problem with standard Dirichlet boundary conditions.

We now observe that $\mathbf{V}_h|_{\Gamma_2} = [W_h]^3$ where W_h is itself a finite element space on the two-dimensional mesh $\mathcal{T}_h^{\Gamma_2}$ induced on Γ_2 by the three-dimensional tessellation \mathcal{T}_h . Remark (see the definition of the space \mathbf{V}) that the functions in W_h satisfy homogeneous boundary conditions on $\partial\Gamma_2$. We then let $\Lambda_h = [W_h]^2$. We consider the following discrete problem:

Problem 3.1. Find $\mathbf{u}_h \in \mathbf{V}_h$, $p_h \in Q_h$, $\boldsymbol{\lambda}_h \in \Lambda_h$ such that for all $\mathbf{v}_h \in \mathbf{V}_h$, $q_h \in Q_h$, $\boldsymbol{\eta}_h \in \Lambda_h$

$$(3.2) \quad 2\mu \int_{\Omega} \mathbf{D}(\mathbf{u}_h) : \mathbf{D}(\mathbf{v}_h) dx - \int_{\Omega} p_h \nabla \cdot \mathbf{v}_h dx - c(\mathbf{v}_h, \boldsymbol{\lambda}_h) = \rho \int_{\Omega} \mathbf{f} \cdot \mathbf{v}_h dx - \int_{\Gamma_2} p_0 \mathbf{n} \cdot \mathbf{v}_h ds,$$

$$(3.3) \quad \int_{\Omega} q_h \nabla \cdot \mathbf{u}_h dx = 0,$$

$$(3.4) \quad c(\mathbf{u}_h, \boldsymbol{\eta}_h) = 0.$$

The following Theorem holds:

Theorem 3.2. There exists h_0 such that, if $h \leq h_0$, Problem 3.1 admits a unique solution $(\mathbf{u}_h, p_h, \boldsymbol{\lambda}_h)$ which verifies

$$\|\mathbf{u}_h\|_{1,\Omega} + \|p_h\|_{0,\Omega} + \|\boldsymbol{\lambda}_h\|_{-1/2,\Gamma_2} \lesssim \|\mathbf{f}\|_{0,\Omega} + \|p_0\|_{0,\Gamma_2}.$$

Moreover the following error estimate holds:

$$\|\mathbf{u} - \mathbf{u}_h\|_{1,\Omega} + \|p - p_h\|_{0,\Omega} \lesssim \inf_{\mathbf{v}_h \in \mathbf{V}_h^0} \|\mathbf{u} - \mathbf{v}_h\|_{1,\Omega} + \inf_{q_h \in Q_h} \|q - q_h\|_{0,\Omega},$$

where

$$\mathbf{V}_h^0 = \{\mathbf{u}_h \in \mathbf{V}_h : c(\mathbf{u}_h, \boldsymbol{\lambda}_h) = 0, \forall \boldsymbol{\lambda}_h \in \Lambda_h\}.$$

Once again, as in the continuous case, the proof of Theorem 3.2 will reduce to prove two inf-sup conditions. We will then start by proving the equivalent of Lemmas 2.6 and 2.7.

Lemma 3.3. It holds that

$$(3.5) \quad \inf_{\boldsymbol{\lambda}_h \in \Lambda_h} \sup_{\mathbf{u}_h \in \mathbf{V}_h} \frac{c(\mathbf{u}_h, \boldsymbol{\lambda}_h)}{\|\boldsymbol{\lambda}_h\|_{-1/2,\Gamma_2} \|\mathbf{u}_h\|_{1,\Omega}} \gtrsim 1.$$

Proof. The key observation that allows us to prove this is that

$$(3.6) \quad B^T [W_h]^3 \subseteq [W_h]^3, \quad B[W_h]^3 \subseteq [W_h]^3.$$

We next observe that we have

$$(3.7) \quad \inf_{\boldsymbol{\lambda}_h \in \Lambda_h} \sup_{\boldsymbol{\eta}_h \in \Lambda_h} \frac{\int_{\Gamma_2} \boldsymbol{\lambda}_h \cdot \boldsymbol{\eta}_h ds}{\|\boldsymbol{\lambda}_h\|_{-1/2,\Gamma_2} \|\boldsymbol{\eta}_h\|_{[H_{00}^{1/2}(\Gamma_2)]^2}} \gtrsim 1.$$

We can prove (3.7) by using Proposition 2.8, Section II.2 in [8]. Adapted to our case, this states that if the inf-sup condition at the continuous level (in our case (2.19)) holds true, a sufficient condition for the validity of the discrete inf-sup condition (3.7) is the existence of a projector $\Pi_h : [H_{00}^{1/2}(\Gamma_2)]^2 \rightarrow \Lambda_h$ verifying

$$\|\Pi_h(\boldsymbol{\eta})\|_{[H_{00}^{1/2}(\Gamma_2)]^2} \lesssim \|\boldsymbol{\eta}\|_{[H_{00}^{1/2}(\Gamma_2)]^2}, \quad \text{and} \quad \int_{\Gamma_2} (\boldsymbol{\eta} - \Pi_h(\boldsymbol{\eta})) \cdot \boldsymbol{\lambda}_h = 0 \quad \forall \boldsymbol{\lambda}_h \in \Lambda_h.$$

We take Π_h as the $[L^2(\Gamma_2)]^2$ projection onto $\Lambda_h \subset [H_0^1(\Gamma_2)]^2$. The quasi-uniformity of the tessellation $\mathcal{T}_h^{\Gamma_2}$ implies that Π_h bounded in $[H_0^1(\Gamma_2)]^2$ (this can be proven by using a global inverse inequality [4]) and, by space interpolation, in $[H_{00}^{1/2}(\Gamma_2)]^2$: $\|\Pi_h \boldsymbol{\eta}\|_{[H_{00}^{1/2}(\Gamma_2)]^2} \lesssim \|\boldsymbol{\eta}\|_{[H_{00}^{1/2}(\Gamma_2)]^2}$. All the assumptions of the above mentioned Proposition are then satisfied, yielding (3.7). Consequently, for any given $\boldsymbol{\lambda}_h \in \Lambda_h$ there exists a $\boldsymbol{\eta}_h \in \Lambda_h$ such that

$$\frac{\int_{\Gamma_2} \boldsymbol{\lambda}_h \cdot \boldsymbol{\eta}_h ds}{\|\boldsymbol{\eta}_h\|_{[H_{00}^{1/2}(\Gamma_2)]^2}} \gtrsim \|\boldsymbol{\lambda}_h\|_{-1/2,\Gamma_2}.$$

We build $\mathbf{u}_h \in \mathbf{V}_h$ as the solution to

$$\int_{\Omega} \nabla \mathbf{u}_h : \nabla \mathbf{v}_h dx = 0 \quad \forall \mathbf{v}_h \in \mathbf{V}_h \cap [H_0^1(\Omega)]^3, \quad \mathbf{u}_h = \mathbf{0} \text{ on } \Gamma_1, \quad \mathbf{u}_h = B^T \begin{pmatrix} \eta_{h,1} \\ \eta_{h,2} \\ 0 \end{pmatrix} \text{ on } \Gamma_2.$$

This equation has a well defined solution since the function which vanishes on Γ_1 and assumes the value $B^T[\eta_{h,1}, \eta_{h,2}, 0]^T$ belongs to $\mathbf{V}_h|_\Gamma$. We observe that

$$\|\mathbf{u}_h\|_{1,\Omega} \simeq \|\mathbf{u}_h\|_{1/2,\Gamma}.$$

From here the proof is identical to the proof of Lemma 2.6. \square

Lemma 3.4. *There exists h_0 such that, if $h \leq h_0$ it holds that*

$$(3.8) \quad \inf_{q_h \in Q_h} \sup_{\mathbf{u}_h \in \mathbf{V}_h^0} \frac{\int_{\Omega} q_h \nabla \cdot \mathbf{u}_h \, ds}{\|\mathbf{u}_h\|_{1,\Omega} \|q_h\|_{0,\Omega}} \gtrsim 1.$$

Proof. In order to prove (3.8) we follow the same reasoning as in the continuous case. Letting $p_h \in Q_h$, we split it as $p_h = p_h^0 + \bar{p}$ with $p_h^0 \in Q_h^0$ and \bar{p} constant. The standard inf-sup condition (3.1) implies the existence of a $\mathbf{u}_h^0 \in \mathbf{V}_h \cap [H_0^1(\Omega)]^3$ ($\subset \mathbf{V}_h^0$), with $\|\mathbf{u}_h^0\|_{1,\Omega} \simeq \|p_h^0\|_{0,\Omega}$ such that

$$\int_{\Omega} p_h^0 \nabla \cdot \mathbf{u}_h^0 \, dx \geq \|p_h^0\|_{0,\Omega}^2.$$

We then build a function $\bar{\mathbf{u}}_h \in \mathbf{V}_h^0$ such that

$$(3.9) \quad \|\bar{\mathbf{u}}_h\|_{1,\Omega} \simeq 1 \quad \text{and} \quad \int_{\Omega} \nabla \cdot \bar{\mathbf{u}}_h \, dx = 1.$$

In order to do so, we let $\bar{\eta}_h \in \mathbf{V}_h|_{\Gamma_2} \cap [H_0^1(\Gamma_2)]^3$ denote the $L^2(\Gamma_2)$ orthogonal projection of $\bar{\mathbf{u}}|_{\Gamma_2}$ (where $\bar{\mathbf{u}}$ is the function introduced in the proof of Lemma 2.7), and we let $\hat{\mathbf{u}}_h \in \mathbf{V}_h$ denote the solution of

$$\int_{\Omega} \nabla(\hat{\mathbf{u}}_h) : \nabla(\mathbf{v}_h) = 0, \quad \forall \mathbf{v}_h \in \mathbf{V}_h \cap [H_0^1(\Omega)]^3, \quad \hat{\mathbf{u}}_h = \bar{\eta}_h \text{ on } \Gamma_2, \quad \hat{\mathbf{u}}_h = \mathbf{0} \text{ on } \Gamma_1.$$

It is not difficult to check that $\hat{\mathbf{u}}_h \in \mathbf{V}_h^0$. In fact we have, for $\lambda_h \in \Lambda_h$:

$$c(\hat{\mathbf{u}}_h, \lambda_h) = \int_{\Gamma_2} [(\hat{\mathbf{u}}_h \cdot \mathbf{t}_1)\lambda_{h,1} + (\hat{\mathbf{u}}_h \cdot \mathbf{t}_2)\lambda_{h,2}] \, ds = \int_{\Gamma_2} (\zeta_{h,1}\lambda_{h,1} + \zeta_{h,2}\lambda_{h,2}) \, ds,$$

where $\zeta_h = B\eta_h$. By the linearity of the $L^2(\Gamma_2)$ projection operator and since B is a constant matrix, we have that ζ_h is the $[L^2(\Gamma_2)]^3$ projection of $\zeta = B\bar{\mathbf{u}}$, which implies

$$c(\hat{\mathbf{u}}_h, \lambda_h) = \int_{\Gamma_2} (\zeta_{h,1}\lambda_{h,1} + \zeta_{h,2}\lambda_{h,2}) \, ds = \int_{\Gamma_2} (\zeta_1\lambda_{h,1} + \zeta_2\lambda_{h,2}) \, ds = \int_{\Gamma_2} [(\bar{\mathbf{u}} \cdot \mathbf{t}_1)\lambda_{h,1} + (\bar{\mathbf{u}} \cdot \mathbf{t}_2)\lambda_{h,2}] \, ds = 0.$$

Moreover we have the following Lemma.

Lemma 3.5. *There exists h_0 such that for all $h \leq h_0$ we have*

$$\|\hat{\mathbf{u}}_h\|_{1,\Omega} \simeq \|\bar{\mathbf{u}}\|_{1,\Omega}, \quad \int_{\Gamma_2} \hat{\mathbf{u}}_h \cdot \mathbf{n} \, ds \simeq 1.$$

Then the function

$$\bar{\mathbf{u}}_h = \hat{\mathbf{u}}_h \left(\int_{\Gamma_2} \hat{\mathbf{u}}_h \cdot \mathbf{n} \, ds \right)^{-1},$$

satisfies (3.9). We control p_h with $\mathbf{u}_h = \mathbf{u}_h^0 + t\bar{p}\bar{\mathbf{u}}_h$. We have

$$\begin{aligned} \int_{\Omega} (p_h^0 + \bar{p}) \nabla \cdot (\mathbf{u}_h^0 + t\bar{p}\bar{\mathbf{u}}_h) \, dx &= \int_{\Omega} p_h^0 \nabla \cdot \mathbf{u}_h^0 \, dx + t\bar{p} \int_{\Omega} p_h^0 \nabla \cdot \bar{\mathbf{u}}_h \, dx + t\bar{p}^2 \int_{\Omega} \nabla \cdot \bar{\mathbf{u}}_h \, dx = \\ &= \int_{\Omega} p_h^0 \nabla \cdot \mathbf{u}_h^0 \, dx + t\bar{p} \int_{\Omega} p_h^0 \nabla \cdot \bar{\mathbf{u}}_h \, dx + t\bar{p}^2 \int_{\Gamma_2} \bar{\mathbf{u}}_h \cdot \mathbf{n} \, ds \geq \|p_h^0\|_{0,\Omega}^2 - \gamma_0 t |\bar{p}| \|p_h^0\|_{0,\Omega} + t\bar{p}^2 \geq \\ &\geq \|p_h^0\|_{0,\Omega}^2 + t\bar{p}^2 - \gamma_0 t \frac{1}{2\varepsilon} \|p_h^0\|_{0,\Omega}^2 - \gamma_0 t \frac{\varepsilon}{2} \bar{p}^2. \end{aligned}$$

We now choose ε in such a way that $\gamma_1 = 1 - \gamma_0\varepsilon/2 > 0$. Once ε is chosen we choose $t > 0$ in such a way that $\gamma_2 = 1 - \gamma_1 t/(2\varepsilon) > 0$. We then obtain

$$\int_{\Omega} (p_h^0 + \bar{p}) \nabla \cdot (\mathbf{u}_h^0 + t\bar{p}\bar{\mathbf{u}}_h) \, dx \geq \gamma_2 \|p_h^0\|_{0,\Omega}^2 + t\gamma_1 \bar{p}^2 \gtrsim \|p_h\|_{0,\Omega}^2.$$

□

Proof of Lemma 3.5. By a standard reasoning it is possible to show that the $L^2(\Gamma_2)$ projection onto $\mathbf{V}_h|_{\Gamma_2} \cap [H_0^1(\Gamma_2)]^3$ is bounded in $[H_{00}^{1/2}(\Gamma_2)]^3$. Then we have

$$\|\hat{\mathbf{u}}_h\|_{1/2,\Gamma} \simeq \|\hat{\mathbf{u}}_h\|_{[H_{00}^{1/2}(\Gamma_2)]^3} \lesssim \|\bar{\mathbf{u}}\|_{[H_{00}^{1/2}(\Gamma_2)]^3} \simeq \|\bar{\mathbf{u}}\|_{1/2,\Gamma}.$$

On the other hand, by triangular inequality we have:

$$\|\bar{\mathbf{u}}\|_{[H_{00}^{1/2}(\Gamma_2)]^3} \leq \|\hat{\mathbf{u}}_h\|_{[H_{00}^{1/2}(\Gamma_2)]^3} + \|\bar{\mathbf{u}} - \hat{\mathbf{u}}_h\|_{[H_{00}^{1/2}(\Gamma_2)]^3}.$$

We now recall that $\bar{\mathbf{u}}$ was chosen in $[H^2(\Omega)]^3$. This allows us to write

$$\|\hat{\mathbf{u}}_h\|_{[H_{00}^{1/2}(\Gamma_2)]^3} \geq \|\bar{\mathbf{u}}\|_{[H_{00}^{1/2}(\Gamma_2)]^3} - \|\bar{\mathbf{u}} - \hat{\mathbf{u}}_h\|_{[H_{00}^{1/2}(\Gamma_2)]^3} \geq \|\bar{\mathbf{u}}\|_{[H_{00}^{1/2}(\Gamma_2)]^3} + Ch\|\bar{\mathbf{u}}\|_{3/2,\Gamma_2}.$$

Since $\bar{\mathbf{u}}$ is a fixed function, chosen once for all, $\|\bar{\mathbf{u}}\|_{3/2,\Gamma_2}$ and $\|\bar{\mathbf{u}}\|_{[H_{00}^{1/2}(\Gamma_2)]^3}$ are two fixed numbers, essentially depending on Ω and Γ_2 , and their ratio

$$\alpha = \frac{\|\bar{\mathbf{u}}\|_{[H_{00}^{1/2}(\Gamma_2)]^3}}{\|\bar{\mathbf{u}}\|_{3/2,\Gamma_2}}$$

is a given constant, for which we can write

$$\|\hat{\mathbf{u}}_h\|_{[H_{00}^{1/2}(\Gamma_2)]^3} \geq (1 - C\alpha h)\|\bar{\mathbf{u}}\|_{[H_{00}^{1/2}(\Gamma_2)]^3}^2.$$

Then, provided $h \leq h_1$ with $h_1 = 1/(2C\alpha)$, we have

$$\|\hat{\mathbf{u}}_h\|_{[H_{00}^{1/2}(\Gamma_2)]^3}^2 \geq \frac{1}{2}\|\bar{\mathbf{u}}\|_{[H_{00}^{1/2}(\Gamma_2)]^3}^2.$$

As far as the second part of our statement is concerned, we have

$$\int_{\Gamma} \hat{\mathbf{u}}_h \cdot \mathbf{n} \, ds = \int_{\Gamma} \bar{\mathbf{u}} \cdot \mathbf{n} \, ds - \int_{\Gamma} (\bar{\mathbf{u}} - \hat{\mathbf{u}}_h) \cdot \mathbf{n} \, ds = 1 - I.$$

On the one hand:

$$1 - I \lesssim 1 + |I| \lesssim 1 + \|\bar{\mathbf{u}} - \hat{\mathbf{u}}_h\|_{0,\Gamma} \leq 1 + Ch^{3/2}\|\bar{\mathbf{u}}\|_{2,\Omega}.$$

Once again, since $\|\bar{\mathbf{u}}\|_{2,\Omega}$ is a fixed number we can introduce the constant

$$\beta = \frac{1}{\|\bar{\mathbf{u}}\|_{2,\Omega}},$$

and we can write

$$\int_{\Gamma} \hat{\mathbf{u}}_h \cdot \mathbf{n} \, ds \leq (1 + Ch\beta) \lesssim 1.$$

As far as the lower bound is concerned we have:

$$\int_{\Gamma} \hat{\mathbf{u}}_h \cdot \mathbf{n} \, ds \geq (1 - Ch\beta).$$

Choosing $h \leq h_2$ with h_2 such that $Ch_2\beta < 1/2$ we get the thesis for $h_0 = \min\{h_1, h_2\}$. □

Proof of Theorem 3.2. The validity of the two inf-sup conditions (3.5) and (3.8) implies the existence, uniqueness and stability part of Theorem 3.2.

In order to derive an error estimate we start by observing that we have $\mathbf{V}_h^0 \subset \mathbf{V}^0$. In fact assuming that $c(\mathbf{u}_h, \boldsymbol{\lambda}_h) = 0, \forall \boldsymbol{\lambda}_h \in \Lambda_h$ and taking $\boldsymbol{\lambda}_h = (\lambda_{h,1}, \lambda_{h,2})$ with $\lambda_{h,1} = \mathbf{u}_h \cdot \mathbf{t}_1 \in W_h$ and $\lambda_{h,2} = \mathbf{u}_h \cdot \mathbf{t}_2 \in W_h$, we obtain

$$\int_{\Gamma_2} (|\mathbf{u}_h \cdot \mathbf{t}_1|^2 + |\mathbf{u}_h \cdot \mathbf{t}_2|^2) \, ds = 0 \quad \Rightarrow \mathbf{u}_h \in \mathbf{V}^0.$$

By applying Proposition 2.4, Chapter 2 in [8], and in particular the estimate (2.12) we have

$$\|\mathbf{u} - \mathbf{u}_h\|_{1,\Omega} + \|p - p_h\|_{0,\Omega} \lesssim \inf_{\mathbf{v}_h \in \mathbf{V}_h^0} \|\mathbf{u} - \mathbf{v}_h\|_{1,\Omega} + \inf_{q_h \in Q_h} \|q - q_h\|_{0,\Omega}.$$

□

Remark 3.6. Remark that there is no reason why the multiplier $i(\lambda) = \tau(\mathbf{u}, p)$ should vanish at the boundary of Γ_2 . Therefore, the proposed discretization cannot, in general, yield an optimal approximation of the Lagrange multiplier. Nevertheless, since $V_h^0 \subset V^0$, the approximation properties for the Lagrange multiplier do not enter the error estimate in Theorem 3.2, and we get an optimal error estimate for both velocity and pressure (see e.g. (4.2)).

Remark 3.7. Throughout Sections 2 and 3 we assumed that Γ_2 was a flat surface (or, more precisely, we assumed that \mathbf{n} was constant on the connected components of Γ_2). Let us consider two cases in which this assumption is not satisfied. If a connected component of Γ_2 is the union of two (or more) flat subregions sharing a vertex (in 2D) or an edge (in 3D), we observe that, at the continuous level, if \mathbf{n}_1 and \mathbf{n}_2 are constant unit normals to the two subregions with direction chosen in such a way that on the common vertex or edge we have $\mathbf{u} = |\mathbf{u}|\mathbf{n}_1 = |\mathbf{u}|\mathbf{n}_2$, if $\mathbf{n}_1 \neq \mathbf{n}_2$ then $\mathbf{u} = 0$, so that the solution vanishes at the interface between the two subregions. At the discrete level one needs then to strongly force the velocity to vanish on such interface. Once this is done, the analysis presented above remains valid.

If, on the other hand, Γ_2 is a curved surface, the situation is more complex. Let us first consider the continuous problem. Theorem 2.3 does not yield $(\sigma(\mathbf{u}, p)\mathbf{n}) \cdot \mathbf{n} = -p$. Though the splitting (2.7) still holds, it does not reduce to (2.8) anymore. The natural boundary condition implicit in equation (2.14) is not (2.5), but rather

$$(3.10) \quad p + 2\mu|\mathbf{u}|\kappa = p_0, \quad \text{on } \Gamma_2.$$

Nevertheless, Problem 2.4 is still well posed, and Theorem 2.5 still holds, provided equation (2.5) is replaced by equation (3.10).

Things are more complex when it comes to discretizing Problem 2.4. In fact, the two inclusions in (3.6) do not generally hold for curved boundaries. In addition, if the normal to the discrete boundary has jumps (which would automatically happen when approximating a curved boundary with a finite element mesh), we do not even have $B(W_h)^3 \subseteq [H_{00}^{1/2}(\Omega)]^3$. The whole method would then be non conforming. Remark that we might also need to resort to a non conforming discretization if we drop the requirement that the tessellation \mathcal{T}_h is compatible with the splitting of $\partial\Omega$ into $\Gamma_1 \cup \Gamma_2$.

4. SOLUTION STRATEGY

4.1. Discretization and algebraic solution. We now turn to the solution strategy. We consider \mathcal{T}_h to be a tetrahedral mesh and we use Taylor-Hood elements, that is, for some $k \geq 2$ we set:

$$\begin{aligned} V_h &= \{\mathbf{u} \in [C^0(\Omega)]^3 : \forall K \in \mathcal{T}_h \mathbf{u}|_K \in [\mathbb{P}^k(K)]^3\}, \\ Q_h &= \{p \in C^0(\Omega) : \forall K \in \mathcal{T}_h p|_K \in \mathbb{P}^{k-1}(K)\}. \end{aligned}$$

It is well known that such elements satisfy the inf-sup condition (3.1), see for instance [8]. Moreover for all $\mathbf{v} \in [H^s(\Omega)]^3$, $1 \leq s \leq k+1$, and for all $q \in H^t(\Omega)$, $0 \leq t \leq k$ we have

$$(4.1) \quad \inf_{\mathbf{v}_h \in V_h} \|\mathbf{v} - \mathbf{v}_h\|_{1,\Omega} \lesssim h^{s-1} \|\mathbf{v}\|_{s,\Omega}, \quad \inf_{q_h \in Q_h} \|q - q_h\|_{0,\Omega} \lesssim h^t \|q\|_{t,\Omega}.$$

Thanks to the planarity of the connected components of Γ_2 , for \mathbf{v} with $\mathbf{v}_{\parallel} = 0$, the infimum in the first bound of (4.1) can be taken over the smaller space V_h^0 without changing the right hand side. Then, thanks to Theorem 3.2, if the solution to Problem 2.4 satisfies $\mathbf{u} \in [H^{k+1}(\Omega)]^3$ and $p \in H^k(\Omega)$, we have

$$(4.2) \quad \|\mathbf{u} - \mathbf{u}_h\|_{1,\Omega} + \|p - p_h\|_{0,\Omega} \lesssim h^k (\|\mathbf{u}\|_{k+1,\Omega} + \|p\|_{k,\Omega}).$$

We thus expect optimal convergence rates provided the solution has sufficient regularity. If this is not the case (as for instance in the case of a Stokes problem with mixed boundary conditions in a nonsmooth domain [28]), we could think of enriching the polynomial approximation spaces we previously used with non-smooth functions in order to deal with the singularities, in the spirit of the XFEM methodology [18]. We believe that the theoretical abstract framework we developed could be easily adapted to such a class of methods.

Let us now consider the corresponding algebraic representation; it reads:

$$(4.3) \quad \begin{pmatrix} A & D^T & E^T \\ D & 0 & 0 \\ E & 0 & 0 \end{pmatrix} \begin{pmatrix} U \\ P \\ \Lambda \end{pmatrix} = \begin{pmatrix} F \\ 0 \\ 0 \end{pmatrix}$$

where A corresponds to the velocity terms, E and E^T the coupling terms between the Lagrange multipliers and the velocity and D, D^T the coupling terms between velocity and pressure. U, P, Λ are respectively the algebraic representation of \mathbf{u}, p, λ . To solve (4.3), we consider three strategies: (i) Strategy P_{GASM} couples monolithically a Krylov iterative solver with an additive Schwarz preconditioner and (ii) Strategy P_1^{BLOCK} and Strategy P_2^{BLOCK} couple a Krylov iterative solver with a block preconditioning strategy.

Regarding strategies P_1^{BLOCK} and P_2^{BLOCK} , we follow the framework proposed in [13] to develop an efficient preconditioner. To apply this framework, we remark that (4.3) can be seen as a double saddle point problem: we gather either the velocity-pressure unknowns and or the velocity-Lagrange multiplier unknowns to setup a two level preconditioner.

Remark 4.1. As mentioned before, it is clear that the Lagrange multiplier formulation described in Problem 2.4 is less straightforward to implement in practice: the main difficulty comes from the double saddle point structure of the problem, that cannot be handled only by a direct use of a Stokes or Navier-Stokes code as a black box. Nevertheless, having a flexible and powerful computational framework which enables advanced numerical methods as described hereafter, this formulation does have several advantages: (i) optimal a priori estimates are available in the natural norms for the problem (ii) no stabilization is being required and hence the formulation requires no tuning parameters as in [7] and (iii) the coupling between the velocity and the Lagrange multiplier λ occurs only on Γ_2 and hence has little impact on the problem size.

4.2. Computational framework. The analysis hereafter is developed in the framework of the Finite Element Embedded Library in C++ (Feel++). Feel++ allows to use a very wide range of Galerkin methods and advanced numerical techniques such as domain decomposition (including mortar and three fields methods), fictitious domain or certified reduced basis. The ingredients include a very expressive embedded language, seamless interpolation, mesh adaption and seamless parallelization. It has been used in various contexts including the development and/or numerical verification of (new) mathematical methods or the development of large multi-physics applications [32, 9]. The range of users spans from mechanical engineers in industry, physicists in complex fluids, computer scientists in biomedical applications to applied mathematicians thanks to the shared common mathematical embedded language hiding linear algebra and computer science complexities.

Feel++ provides a mathematical kernel for solving partial differential equation using arbitrary order Galerkin methods (FEM, SEM, CG, DG, CRB) in 1D, 2D, 3D and on manifolds using simplices and hypercubes meshes [31]: (i) a polynomial library allowing for a wide range polynomial expansions including H_{div} and H_{curl} elements, (ii) a light interface to Boost.UBLAS, EIGEN3 and PETSc[3]/SLEPc as well as a scalable in-house solution strategy (iii) a language for Galerkin methods starting with fundamental concepts such as function spaces, forms, operators, functionals and integrals, (iv) a framework that allows user codes to scale seamlessly from single core computation to thousands of cores and enables hybrid computing.

Regarding the specific implementation with Feel++ of the proposed methodology, we would like to point out some non-standard aspects, namely the treatment of the terms associated to the Lagrange multipliers. Feel++ provides a mechanism to extract submeshes of faces and keep a relation between the extracted mesh and the parent mesh. The relation is necessary to ensure an efficient treatment of the coupling terms between the velocity and the Lagrange multipliers. The geometrical data, *i.e* the normals, are automatically deduced from the parent mesh.

Regarding the implementation of the three strategies described in 4.1, we use the PETSc interface developed in Feel++ and in particular we use the FieldSplit preconditioning framework to implement the block preconditioners strategies.

5. NUMERICAL RESULTS

In this section we evaluate the performances of the method proposed in Section 2.2 and Section 3 when solving two types of problems. First, we construct a manufactured solution in a simple three-dimensional domain and

we assess the convergence properties of the method for different choices of finite elements, by performing a standard mesh refinement study. In addition, we investigate the particular case of a Stokes flow in a tube with Γ_2 aligned to an axis and explore the capabilities of the method when applied in a case when Γ_2 is curved. Second, we implement this new approach in a complex application, namely to compute the solution to a three-dimensional computational model of the cerebral venous blood flow that we described in Section 2.1.

Problem 1: Stokes flow in a curved tube. We start by checking numerically the convergence properties of the method by means of a comparison with an analytical solution on a curved geometry, namely a torus sector with square cross-section.

The geometry is built as follows: (i) we consider a disk D with inner radius r_1 and outer radius r_2 then (ii) we extract a section S of angle $\theta = \alpha_2 - \alpha_1$ such that at least one of the boundary is not aligned with one of the main axis, e.g. $\frac{\pi}{3}, \frac{\pi}{6}$ and finally (iii) we extrude in the z direction to obtain Ω such that the cross-section is a square of side length $R = r_2 - r_1$. We display in Figure 2 an example of geometry with $r_1 = 1.9$ and $r_2 = 2.1$, $\theta = \frac{\pi}{6}$ and $R = 0.2$: Γ_1 corresponds to the lateral boundary and Γ_2 corresponds to the square surfaces at the extremities of the torus, as shown in Figure 2.

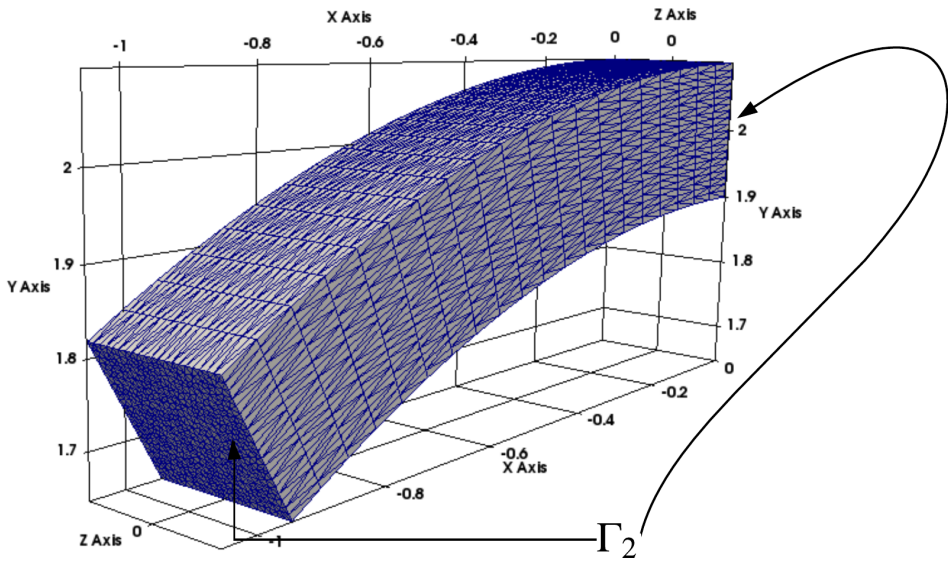


FIGURE 2. Torus sector with square cross-section.

The analytical solution is computed according to the following steps: (i) we first consider the Stokes equations on the section S as in (2.1 - 2.5) (ii) we next analytically solve in polar coordinates (r, θ) the mass and momentum equations with given boundary conditions and finally (iii) the above solution is extruded in the z direction and we impose the exact solution on upper and lower sides in z . Note that we are not exactly in the case of Equations (2.1 - 2.5), since the velocity is non-zero on the lower and upper sides in the z direction. However, this can be dealt with in a standard way by means of a suitable lifting as explained for instance in [14, Section 3.2.2] without impacting the theory.

The explicit expressions for the exact solution, in the case where the angle α_2 corresponds to the inflow section and the angle α_1 corresponds to the outflow section respectively, can be therefore written as follows:

$$(5.1) \quad p_{ex}(r, \theta, z) = \frac{p_{in}(\theta - \alpha_1) + p_{out}(\alpha_2 - \theta)}{\alpha_2 - \alpha_1},$$

$$(5.2) \quad \mathbf{u}_{ex}(r, \theta, z) = [0, \frac{p_{in} - p_{out}}{\alpha_2 - \alpha_1} (\frac{1}{2} r \ln(r) + C \frac{1}{r} + Dr), 0]^T,$$

where

$$C = \frac{1}{2} r_1^2 r_2^2 \frac{\ln(r_1) - \ln(r_2)}{r_1^2 - r_2^2}, \quad D = -\frac{1}{2} \frac{r_1^2 \ln(r_1) - r_2^2 \ln(r_2)}{r_1^2 - r_2^2}.$$

The results presented in the sequel are obtained for $\mu = 1$, when imposing $p_{in} = 10$ at inflow and $p_{out} = 1$ at outflow (we use adimensional units). Figure 3 displays velocity and pressure solution profiles in the torus geometry for $\theta = \frac{\pi}{6}$, showing a Poiseuille-like profile for the velocity and a constant pressure field on each cross-section, correctly enforced at both inflow and outflow section. Figure 4 displays the order of the spatial discretization error as a function of the mesh size h for $\theta = \frac{\pi}{6}$ on the 3D torus geometry described above. The convergence rates expected by (4.2) are obtained.

Figure 5 plots the velocity and pressure errors with respect to (i) the number of non-zero entries (nnz) in the matrix associated to the discretization of problem 2.5 (ii) the number of velocity and pressure unknowns and (iii) the number of Lagrange multiplier unknowns. It gives some insight into the error versus memory/computational cost of the methodology proposed and the chosen approximation parameters. We recall that (i) the Lagrange multipliers have little impact on the problem size since they are defined only on Γ_2 hence $\dim \Lambda_h \ll \{\dim V_h, \dim Q_h\}$ and (ii) the Lagrange multipliers do not play any role in the *a priori* error estimates (4.2).

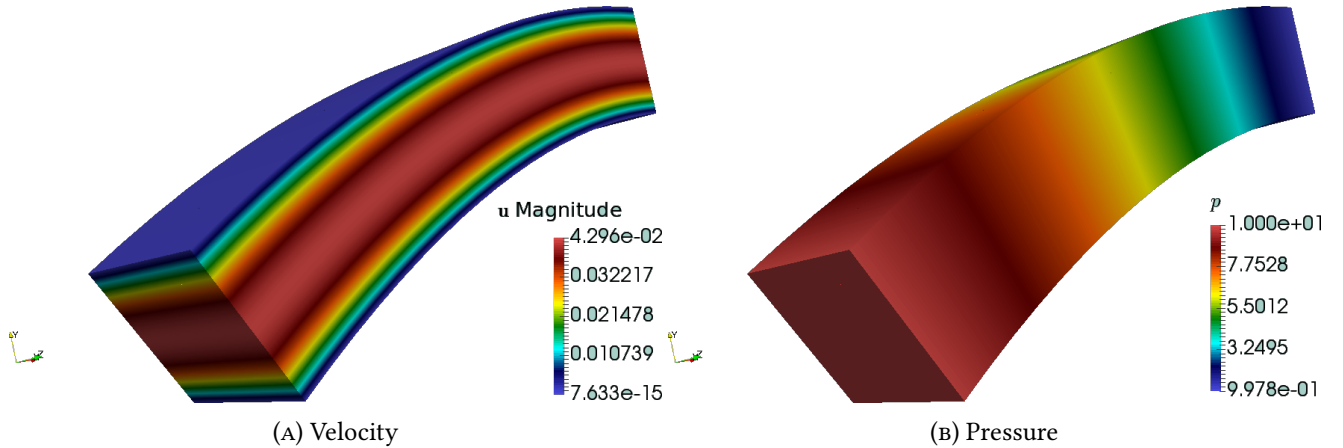


FIGURE 3. Torus geometry for $\theta = \frac{\pi}{6}$: velocity and pressure profiles.

Stokes flow in a tube with Γ_2 aligned to an axis. In the case where Γ_2 is aligned to an axis, there is no need to use the Lagrange multiplier formulation. Indeed, it suffices to set to 0 the tangential components of \mathbf{u} which correspond to the components orthogonal to the axis Γ_2 is aligned to. For example, if Γ_2 is aligned to the X axis, the Y and Z components of \mathbf{u} are set to 0 strongly. Note however that the pressure is still imposed weakly, $p \in L^2(\Omega)$. As a comparison, Figure 6 illustrates a Poiseuille flow in a rectangular domain with the classical *do nothing* condition at the outflow (left panel) and with the boundary conditions set as above (right panel).

Stokes flow in a tube with curved Γ_2 . As discussed in Section 3, at the continuous level, the natural boundary condition applied on a curved boundary takes the form $p + 2\mu|\mathbf{u}|k = p_0$, on Γ_2 . Consequently, it is not the pressure *per se* that is imposed: a Robin-like condition appears in the formulation, in which the curvature of Γ_2 plays a role. In order to investigate the influence of the curvature, we performed a series of two-dimensional numerical tests in a domain Ω constructed as before: we consider a disk D with inner radius r_1 and outer radius r_2 , then we extract a section S of angle $\theta = \frac{\pi}{12}, \frac{\pi}{6}, \frac{\pi}{3}, \frac{2\pi}{3}$. The non-standard boundary condition is not applied on the straight part of the boundary anymore, but on the curved inner part $p_{in} = 10$ and outer part $p_{out} = 1$,

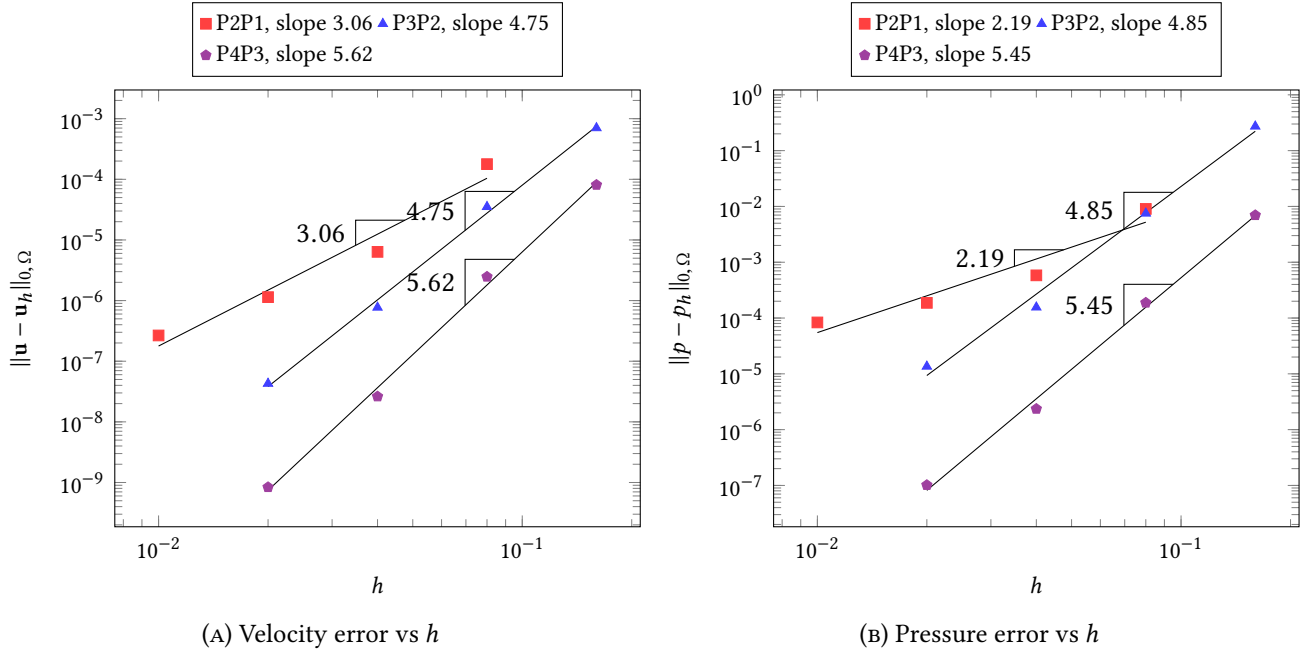


FIGURE 4. Torus geometry for $\theta = \frac{\pi}{6}$: logarithmic plots of the errors for the velocity and pressure, as functions of the mesh size.

respectively, together with the rest of the previously described boundary conditions. Results for the different angles are presented in Figure 7: velocity in the right panel and pressure in the left panel, for $\theta = \frac{\pi}{12}, \frac{\pi}{6}, \frac{\pi}{3}$ and $\frac{2\pi}{3}$, respectively. Interestingly, although the stability and convergence results obtained in Section 3 do not apply in this case, as discussed in Remark 3.7, we still get promising results when applying our method. The velocity profile qualitatively shows a Poiseuille-like profile and no tangential flow on the curved boundaries, in a coherent manner with the imposed condition. The pressure field displays decreasing values, as expected, and show the increasing impact of the curvature term. Further theoretical and numerical investigations are therefore needed in order to adapt the method and we plan at developing this encouraging preliminary study in a forthcoming work.

Problem 2: physiological flow in a realistic geometry. We now consider a more realistic context, an application to hemodynamics, which complements a previous work we developed in [9] on blood flow computational modeling in the cerebral venous network.

We use medical images from the VIVABRAIN project and we use the ANGIOTK platform [1] to construct five different levels of refinement of the computational mesh generated from the MRI images. The characteristics of the meshes $\{M_i\}_{i=0}^4$ are described in Table 1, together with the number of degrees of freedom of the problem when using a stable $\mathbb{P}^2\mathbb{P}^1$ Taylor-Hood spatial discretization.

	h_{min}	h_{max}	$h_{average}$	N_{elt}	N_{dof}
M0	0.104	3.702	0.840	775 242	3 777 309
M1	0.083	3.060	0.697	1 234 148	5 886 029
M2	0.071	2.784	0.607	1 840 209	8 596 453
M3	0.050	2.190	0.478	3 528 238	16 086 516
M4	0.047	1.940	0.408	5 441 080	24 456 367

TABLE 1. Meshes of the cerebral venous network: $h_{min}, h_{max}, h_{average}$ are respectively the minimum, maximum and average edge length in the meshes, N_{elt} is the number of tetrahedra and N_{dof} is the number of degrees of freedom for velocity and pressure.

We consider blood to be a Newtonian fluid with dynamic viscosity $\mu = 3.4815 \cdot 10^{-3}$ [Pa · s] and an external force $\mathbf{f} = \mathbf{0}$. Pressure drop values reported in the clinical literature are quite scarce and it is currently difficult to

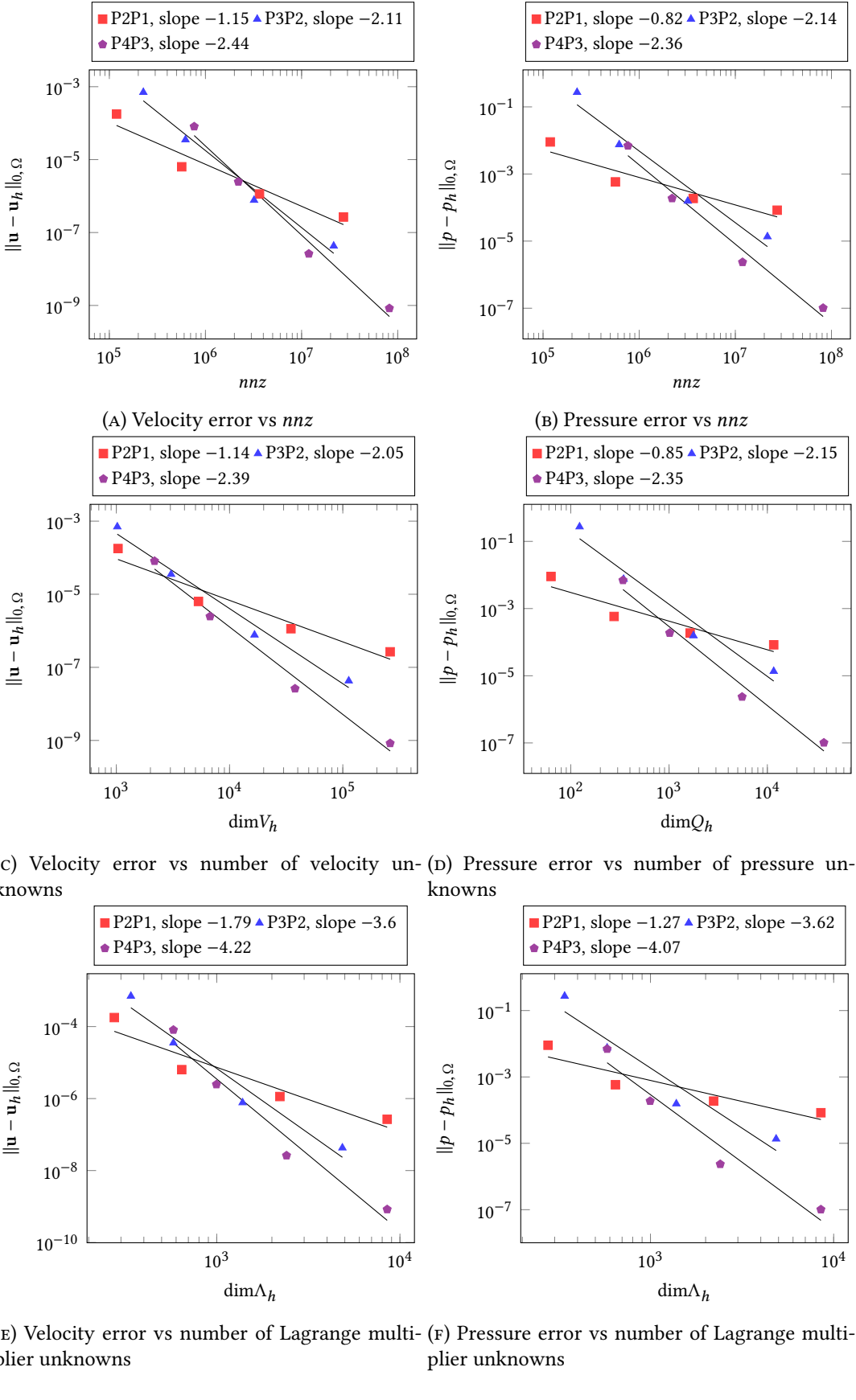
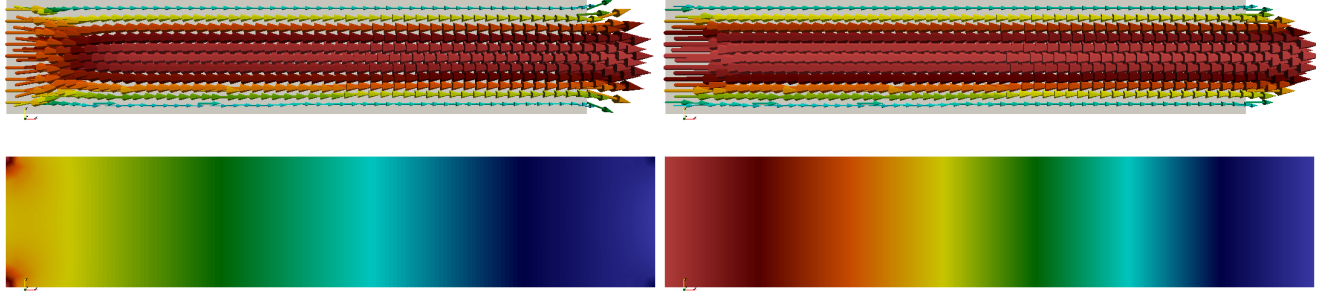


FIGURE 5. Torus geometry for $\theta = \frac{\pi}{6}$: logarithmic plots of the errors for the velocity and pressure, as functions of the number of non-zero entries in the matrix, the number of velocity, pressure and Lagrange multiplier unknowns



(A) Velocity (top) and Pressure (bottom) with *free* boundary conditions (B) Velocity (top) and Pressure (bottom) with *pressure* boundary conditions

FIGURE 6. Poiseuille flow in a straight tube.

find precise figures; the following values extracted from a recent study [19] were used as guidelines: P_{vs} (pressure in the venous sinuses) = 6 mmHg, P_{jl3} (pressure in the upper segment of the left jugular vein) = 5.85 mmHg, P_{jr3} (pressure in the upper segment of the right jugular vein) = 5.85 mmHg. Consequently, we impose the following boundary conditions when solving the Stokes system: (i) $p = 6.75$ mmHg on the inlet sections connected to the superior sagittal sinus; (ii) $p = 6.58$ mmHg on the inlet sections connected to the straight sinus; (iii) $p = 5.85$ mmHg on the right outlet sections and $p = 6.14$ mmHg on the left outlet, together with the condition of no tangential flow on these boundaries; and (iv) $\mathbf{u} = \mathbf{0}$ on the lateral walls.

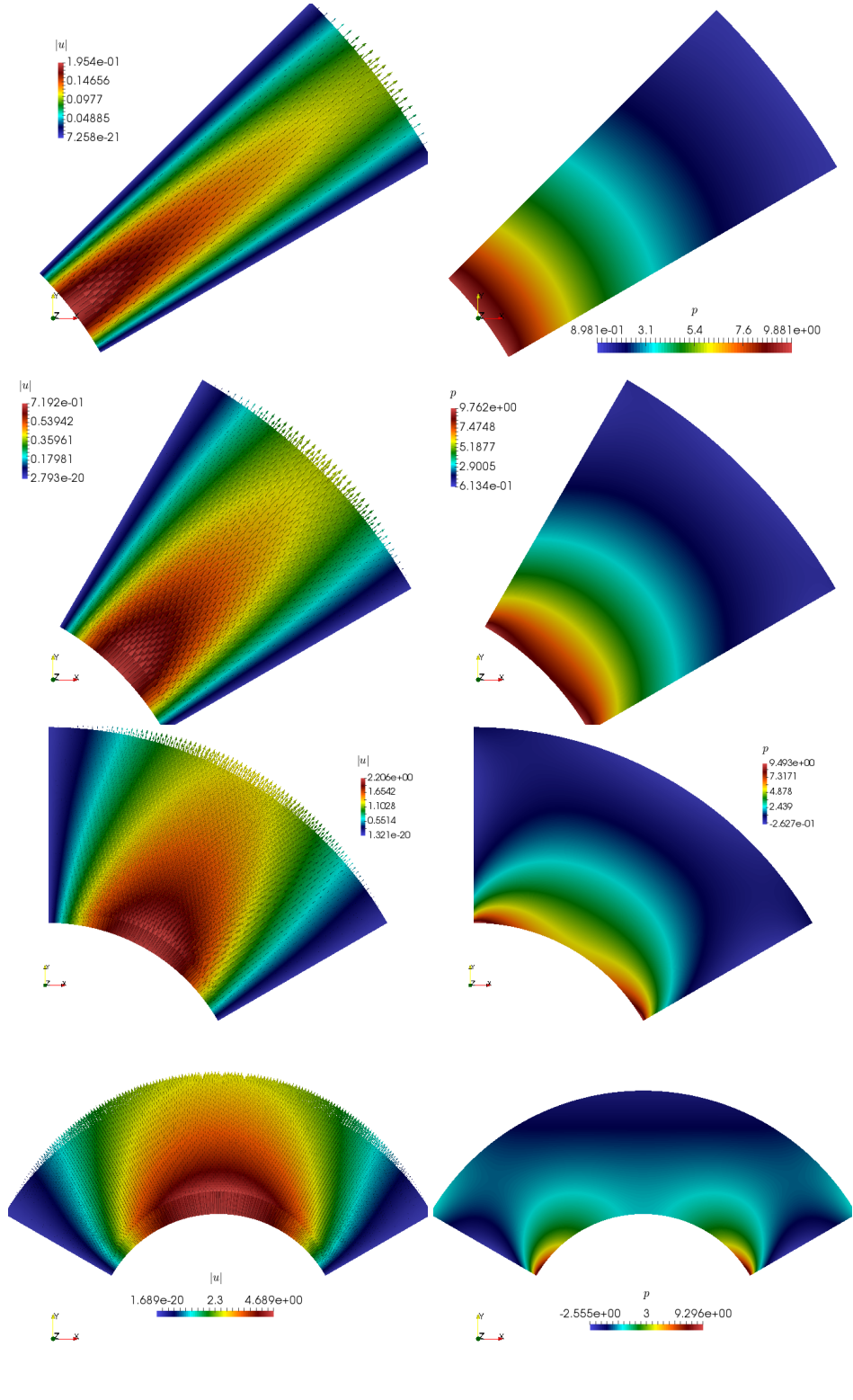
Figure 8 displays the pressure field (left panel) and instantaneous streamlines, colored with velocity magnitude (right panel), illustrating the pressure drop effect and a complicated three-dimensional flow behavior. A zoom on some inlet, respectively outlet sections is presented in Figure 9, demonstrating that the flow is normal to both inflow and outflow surfaces. We highlight the interest of imposing the pressure value and the zero tangential component of the velocity in this context: the current formulation allows to retrieve a Poiseuille-like behavior that is physically meaningful when dealing with artificial boundary conditions, while keeping the viscous stress tensor in the expression of the Stokes problem, useful from a modeling standpoint. The order of magnitude of the maximum velocity is slightly higher than values retrieved in the clinical literature, see for instance [33], therefore more precise values need to be included in further work. However, the development of a computational model able to capture, to this level of accuracy, different features of the flow can be seen as a very promising approach for analyzing, by means of numerical simulations, the dynamics of flow patterns in morphologically complex vascular districts.

The results of the mesh convergence study are displayed in Table 2, showing satisfactory agreement on flow rates and mean pressure value when decreasing the mesh size. Note that an asymmetric behavior of the venous flow appears, equally showed in [27], that could be explained, at least partly, by the asymmetric architecture of the venous network.

	FlowRate0 [m^3/s]	FlowRate1 [m^3/s]	MeanPressure [mmHg]
M0	$4.24732 \cdot 10^{-6}$	$3.18926 \cdot 10^{-6}$	6.51364
M1	$4.27849 \cdot 10^{-6}$	$3.20839 \cdot 10^{-6}$	6.51337
M2	$4.29280 \cdot 10^{-6}$	$3.21806 \cdot 10^{-6}$	6.51328
M3	$4.31223 \cdot 10^{-6}$	$3.23130 \cdot 10^{-6}$	6.51314
M4	$4.31968 \cdot 10^{-6}$	$3.23678 \cdot 10^{-6}$	6.51309

TABLE 2. Mesh refinement effect: FlowRate0 and FlowRate1 correspond to the flow rate on each outlet section, MeanPressure is evaluated on the whole mesh.

Finally, to give an insight about the importance of the preconditioning strategy when solving complex flow problems, we gather in Table 3 results allowing a direct comparison between three possible choices in term of



(A) Velocity.

(B) Pressure.

FIGURE 7. Computational domain for $\theta = \frac{\pi}{12}, \frac{\pi}{6}, \frac{\pi}{3}$ and $\frac{2\pi}{3}$, respectively. Velocity and pressure profiles.

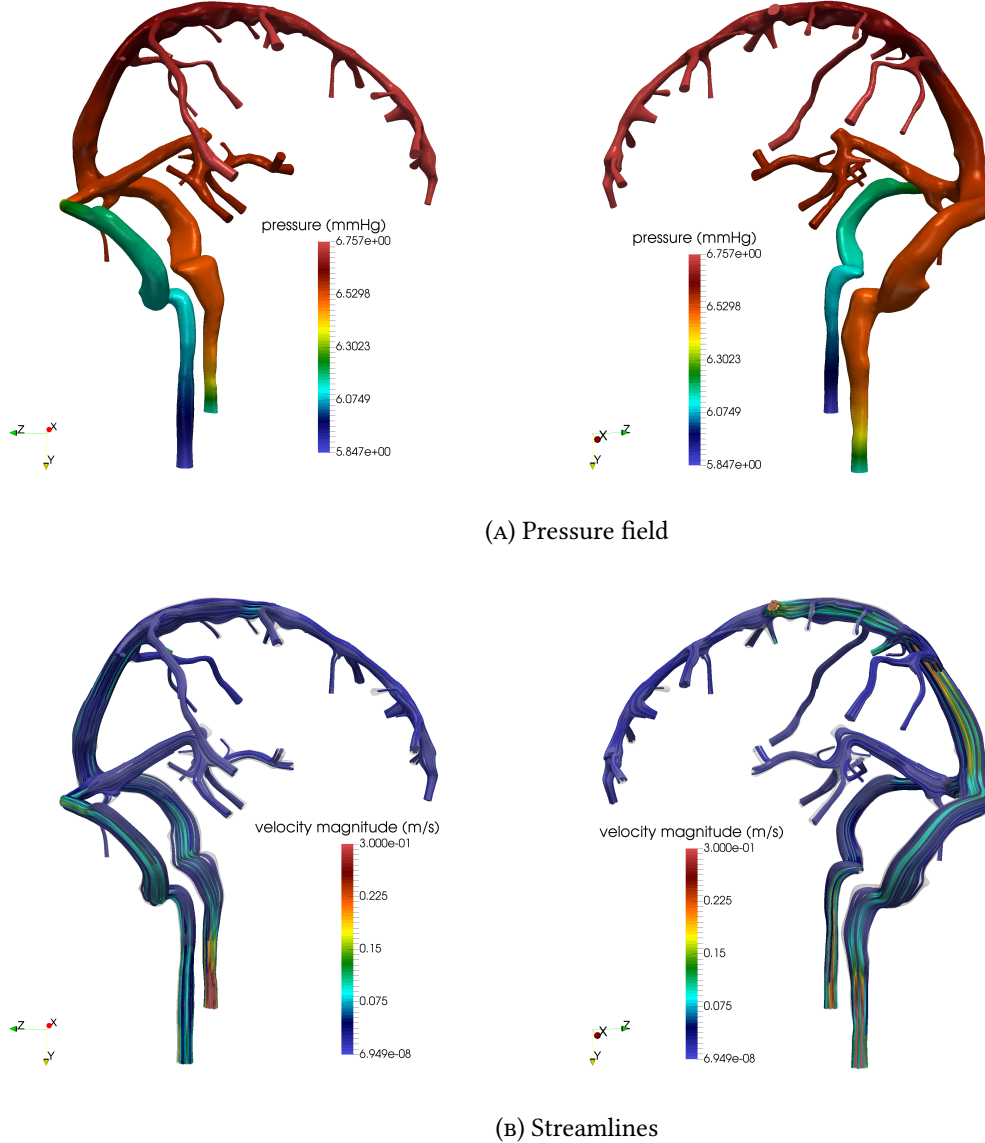


FIGURE 8. Cerebral venous hemodynamics obtained by imposing a pressure drop between the inlet and outlet sections

preconditioners, described in Section 4. Simulations were performed with 96 processors and the time is measured in seconds. The comparison clearly shows the limits of Strategy P^{GASM} and the gain in terms of computational time when choosing Strategy P_1^{BLOCK} and Strategy P_2^{BLOCK} . Note that in the Strategy P_1^{BLOCK} the number of iterations grows strongly with respect to the problem size. Further refinements regarding the different choices are required and will be subject of future research.

6. CONCLUSION AND FUTURE DIRECTIONS

The objective of the present work is to propose a novel formulation for the Stokes problem with non standard boundary conditions prescribing pressure values, together with the condition of no tangential flow, on a part of the boundary. The variational problem, based on a Lagrange multiplier formulation, is shown to be well-posed in the same functional framework as for standard boundary conditions. Moreover, under suitable regularity assumptions, we prove that a strong solution to the initial Stokes problem can be retrieved thanks to this formulation. Next, we consider finite element discretizations, that we analyze, proving that optimal convergence rates can

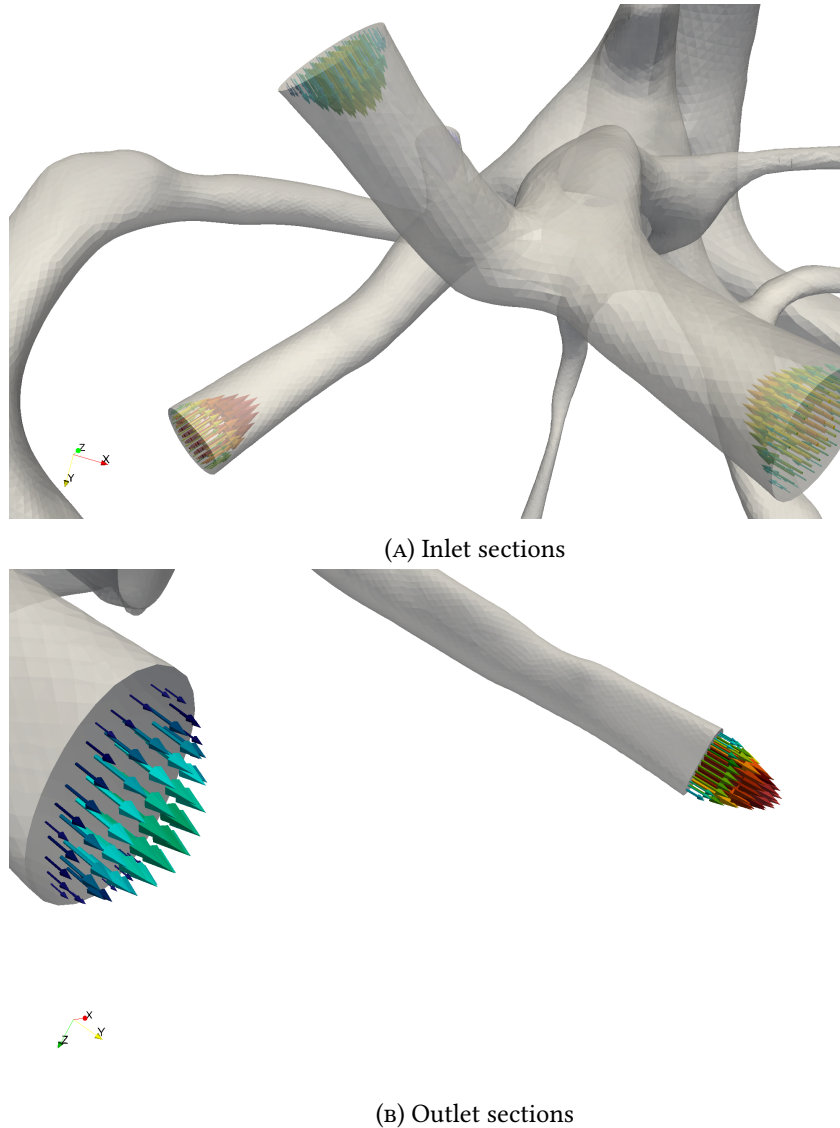


FIGURE 9. Velocity vectors at some inlet, respectively outlet sections.

	Strategy P^{GASM}	Strategy P_1^{BLOCK}	Strategy P_2^{BLOCK}
M0	163[420]	20[174]	67[86]
M1	366[393]	45[267]	161[123]
M2	1080[429]	84[369]	271[143]
M3	4616[522]	293[660]	707[196]
M4	x	898[791]	1960[175]

TABLE 3. Time comparison for three preconditioning strategies implemented in Problem 2 (in seconds). In brackets, the number of iteration used by solver.

be attained for standard inf-sup stable finite element spaces, such as Taylor-Hood elements. Different algebraic solution strategies are proposed including block factorization based preconditioners. Finally, two numerical experiments are performed: the first one numerically illustrates the converge properties of the method and the second one shows the interest of the proposed formulation in a realistic application, namely blood flow modeling of the cerebral vascular network.

The current methodology should be further developed, in particular by (i) devising an adapted discretization strategy for the case of a curved boundary, in order to overcome the difficulties briefly discussed in Section 3; (ii) improving linear solvers scalability by means of well-suited block-preconditioning strategies in the spirit of [13]; (iii) extending the present analysis to the incompressible Navier-Stokes equations and to Generalized non-Newtonian models in the context of blood flow modeling described in [15, Chap. 6]. Furthermore, an exploration of the close connection between Lagrange multipliers technique and a classical method by Nitsche as suggested in [34] provides a promising perspective of the present work.

Finally, simulating blood flow in the cerebral venous network when subject to a physiological pressure gradient gave relevant and interesting results. In view of these findings and targeting the validation of the results with respect to experiments, we aim at including more data at different levels: (i) geometrical description of the network; (ii) mechanical parameters; (iii) more precise measures at the inflow/outflow boundaries, as predominant factors pointed out in [9].

ACKNOWLEDGMENTS

We wish to thank Frédéric Hecht and Mourad Ismail for the fruitful discussions we had. Moreover Vincent Chabannes, Christophe Prud'homme and Marcela Szopos would like to acknowledge the support of (i) Center of Modeling and Simulation of Strasbourg (Cemosis), (ii) Agence Nationale de la Recherche [grant number ANR-12-MONU-0010]. (iii) the LabEx IRMIA and (iv) PRACE for awarding us access to resource Curie based in France at CCRT as well as GENCI for awarding us access to resource Occigen based in France at Cines. Finally Silvia Bertoluzza was supported by Project MIUR-PRIN 2012 (2012HBLYE4) "Innovative Methodologies for PDE based numerical modeling".

REFERENCES

1. *Angiotk project*, <http://www.cemosis.fr/projects/angiotk/>, Accessed: 2016-09-30.
2. C. Amrouche and N. El H. Seloula, *L^p -theory for the Navier-Stokes equations with pressure boundary conditions*, Discrete Contin. Dyn. Syst. Ser. S **6** (2013), no. 5, 1113–1137.
3. S. Balay, S. Abhyankar, M. F. Adams, J. Brown, P. Brune, K. Buschelman, L. Dalcin, V. Eijkhout, W. D. Gropp, D. Kaushik, M. G. Knepley, L. Curfman McInnes, K. Rupp, B. F. Smith, S. Zampini, H. Zhang, and H. Zhang, *PETSc users manual*, Tech. Report ANL-95/11 - Revision 3.7, Argonne National Laboratory, 2016.
4. R.E. Bank and T. Dupont, *An optimal order process for solving finite element equations*, Mathematics of Computation **36** (1981), 35–51.
5. W.L. Barth and G. F. Carey, *On a boundary condition for pressure-driven laminar flow of incompressible fluids*, Internat. J. Numer. Methods Fluids **54** (2007), no. 11, 1313–1325.
6. C. Bègue, C. Conca, F. Murat, and O. Pironneau, *A nouveau sur les équations de Stokes et de Navier-Stokes avec des conditions aux limites sur la pression*, Comptes rendus de l'Académie des sciences. Série 1, Mathématique **304** (1987), no. 1, 23–28.
7. C. Bernardi, T. Chacón Rebollo, and D. Yakoubi, *Finite element discretization of the Stokes and Navier-Stokes equations with boundary conditions on the pressure*, SIAM Journal on Numerical Analysis **53** (2015), no. 3, 1256–1279.
8. F. Brezzi and Fortin M., *Mixed and hybrid finite element methods*, vol. 15, Springer Science & Business Media, 2012.
9. V. Chabannes, M. Ismail, C. Prud'homme, and M. Szopos, *Hemodynamic simulations in the cerebral venous network: A study on the influence of different modeling assumptions*, Journal of Coupled Systems and Multiscale Dynamics **3** (2015), no. 1, 23–37.
10. T. Chacón Rebollo, V. Girault, F. Murat, and O. Pironneau, *Analysis of a coupled fluid-structure model with applications to hemodynamics*, SIAM Journal on Numerical Analysis **54** (2016), no. 2, 994–1019.
11. C. Conca, F. Murat, and O. Pironneau, *The Stokes and Navier-Stokes equations with boundary conditions involving the pressure*, Japanese journal of mathematics. New series **20** (1994), no. 2, 279–318.
12. C. Conca, C. Pares, O. Pironneau, and M. Thiriet, *Navier-Stokes equations with imposed pressure and velocity fluxes*, International journal for numerical methods in fluids **20** (1995), no. 4, 267–287.
13. H. C. Elman, D. J. Silvester, and A. J. Wathen, *Finite elements and fast iterative solvers: with applications in incompressible fluid dynamics*, Oxford University Press (UK), 2014.
14. A. Ern and J.-L. Guermond, *Theory and practice of finite elements*, vol. 159, Springer Science & Business Media, 2013.
15. L. Formaggia, A. Quarteroni, and A. Veneziani, *Cardiovascular mathematics, volume 1 of ms&a. modeling, simulation and applications*, 2009.
16. L. Formaggia and C. Vergara, *Prescription of general defective boundary conditions in fluid-dynamics*, Milan Journal of Mathematics (2012), 1–18.
17. J. Fouchet-Incaux, *Artificial boundaries and formulations for the incompressible Navier-Stokes equations: applications to air and blood flows*, SeMA Journal **64** (2014), no. 1, 1–40.
18. T.-P. Fries and T. Belytschko, *The extended/generalized finite element method: An overview of the method and its applications*, International Journal for Numerical Methods in Engineering **84** (2010), no. 3, 253–304.

19. G. Gadda, A. Taibi, F. Sisini, M. Gambaccini, P. Zamboni, and M. Ursino, *A new hemodynamic model for the study of cerebral venous outflow*, American Journal of Physiology-Heart and Circulatory Physiology **308** (2015), no. 3, H217–H231.
20. V. Girault, *Curl-conforming finite element methods for navier-stokes equations with non-standard boundary conditions in \mathbb{R}^3* , The Navier-Stokes Equations Theory and Numerical Methods, Springer, 1990, pp. 201–218.
21. K.P. Gostaf and O. Pironneau, *Pressure boundary conditions for blood flows*, Chinese Annals of Mathematics, Series B **36** (2015), no. 5, 829–842.
22. Rannacher R. Heywood, J.G. and Turek S., *Artificial boundaries and flux and pressure conditions for the incompressible navier-stokes equations.*, International Journal for Numerical Methods in Fluids **22** (1996), 325–352.
23. S. M. Hosseini and J. J. Feng, *Pressure boundary conditions for computing incompressible flows with SPH*, Journal of Computational physics **230** (2011), no. 19, 7473–7487.
24. H. Johnston and J.-G. Liu, *Finite difference schemes for incompressible flow based on local pressure boundary conditions*, Journal of Computational Physics **180** (2002), no. 1, 120–154.
25. J.M. Leone and P. M. Gresho, *Finite element simulations of steady, two-dimensional, viscous incompressible flow over a step*, Journal of Computational Physics **41** (1981), no. 1, 167–191.
26. S. Marušić, *On the Navier-Stokes system with pressure boundary condition*, Annali Univ. Ferrara **53** (2007), no. 2, 319–331.
27. O. Miraucourt, S. Salmon, M. Szopos, and M. Thiriet, *Blood flow in the cerebral venous system: modeling and simulation*, Computer methods in biomechanics and biomedical engineering **20** (2017), no. 5, 471–482.
28. M. Orlt and A.-M. Sändig, *Regularity of viscous Navier-Stokes flows in nonsmooth domains*, Boundary value problems and integral equations in nonsmooth domains (Luminy, 1993) **167** (1994), 185–201.
29. O. Pironneau, *Conditions aux limites sur la pression pour les équations de Stokes et de Navier-Stokes*, C. R. Acad. Sci. Paris Sér. I Math. **303** (1986), no. 9, 403–406.
30. Vergara C. Porpora A., Zunino P. and Piccinelli M., *Numerical treatment of boundary conditions to replace lateral branches in hemodynamics*, International journal for numerical methods in biomedical engineering **28** (2012), no. 12, 1165–1183.
31. C. Prud'Homme, V. Chabannes, V. Doyeux, M. Ismail, A. Samake, and G. Pena, *Feel++: A Computational Framework for Galerkin Methods and Advanced Numerical Methods*, ESAIM: Proc. **38** (2012), 429 – 455.
32. C. Caldini Queiros, V. Chabannes, M. Ismail, G. Pena, C. Prud'Homme, M. Szopos, and R. Tarabay, *Towards large-scale three-dimensional blood flow simulations in realistic geometries*, ESAIM Proc. **43** (2013), 195–212.
33. B. Schaller, *Physiology of cerebral venous blood flow: from experimental data in animals to normal function in humans*, Brain research reviews **46** (2004), no. 3, 243–260.
34. Rolf Stenberg, *On some techniques for approximating boundary conditions in the finite element method*, Journal of Computational and applied Mathematics **63** (1995), no. 1, 139–148.
35. C. Vergara, *Nitsche's method for defective boundary value problems in incompressible fluid-dynamics*, Journal of Scientific Computing **46** (2011), no. 1, 100–123.